GEOFF CLARKE, PHD., POSTDOCTORAL FELLOW,
UNIVERSITY OF TORONTO, DEPARTMENT OF MEDICINE

October 29, 2005

Dr. Yves Brun,
Systems Biology/Microbiology Faculty Search,
Department of Biology,
Indiana University,
Jordan Hall 142,
1001 E 3rd St,
Bloomington IN
47405-7005

Dear Dr Brun, and the Search Committee:

My name is Geoff Clarke, and I'm currently a postdoctoral fellow at the University of Toronto. I'm writing to you in regards to the tenure track positions that have been advertised by the Department of Biology and the Biocomplexity Institute at Indiana University. I'd like to take this opportunity to introduce myself, and to tell you a little about my background with the hope of discussing the possibility of joining the department as an Assistant Professor.

I completed my bachelors degree in Biology at the University of Guelph, Ontario,, and went on to complete a PhD at the University of Toronto. During my doctoral studies, I analyzed the *in vivo* function of the rod photoreceptor-specific protein Rom-1 and was able to demonstrate, among other things, that Rom-1 was critical to the viability of rod photoreceptor, thereby establishing it as a causative factor in the group of inherited retinopathies known as retinitis pigmentosa. I also performed a computational analysis of the kinetics of neurodegenerative cell loss kinetics, and made the important and controversial observation that affected neurons exhibit a constant risk of dying throughout their lifetime. I then began a CIHR fellowship at the University of Toronto, where I began to study the techniques of theoretical and computational biology, and have recently used them to demonstrate that cell death kinetics are consistent with a power-law distribution of death risk across affected populations. Recently I was involved with the characterization of proteins involved in the muscle cell insulin response, and have begun computational analysis of the muscle and adipose cell insulin signaling networks. In the future, I plan to continue analyzing models of neurodegenerative cell loss, including an exploration of the role of stochastic biochemical fluctuations in regulating apoptotic commitment, as well as studying models of insulin signaling in peripheral tissues with the goal of understanding the etiology of insulin resistance and type 2 diabetes.

My research experience to date has given me an opportunity to learn techniques from a wide range of traditional disciplines, including molecular biology, biochemistry, theoretical and computational biology. Considering that the high-throughput techniques of cellular and molecular biology promise to dramatically increase our quantitative knowledge of the molecules involved in various biological processes, I believe we have entered a period in which advancing our understanding of living systems is limited only by our ability to organize and interpret this

new wealth of data. Consequently, it is becoming increasingly important for biologist to understand and utilize not only the traditional tools of experimental biology, but also the variety of computational tools that are now being used in the exploration of living systems. I feel that my background and experience in both areas of research will not only allow me to perform independent multidisciplinary research, but will also allow me to facilitate the interaction between researchers from traditional academic fields. As such, I feel this makes me an ideal candidate for the faculty position associated with the Department of Biology and the Biocomplexity Institute.

I greatly look forward to discussing with you the possibility of my joining Indiana University.

Sincerely,

Geoff Clarke
Postdoctoral Fellow
University of Toronto
Department of Medicine
Medical Sciences Building, Room 7313
1 King's College Circle
Toronto, On
M5G 1X8
Phone: 416-978-1699
Fax: 416-978-3701
Email: geoff.clarke@utoronto.ca

Geoffrey A. Clarke, Ph.D.
Curriculum Vitae

Business Address

University of Toronto
Department of Medicine
Medical Sciences Building
Room 7313,
1 King's College Circle
Toronto, Ontario
M5S 1A8
Phone: (416) 978-1699
Fax: (416) 978-3701
geoff.clarke@utoronto.ca

Contact Address

93 Wiley Ave
Toronto, Ontario
M4J 3W5
Canada
Phone: (416)778-6972

Education

1986 - 1989 Bachelor of Science University of Toronto
Specialist Program in Zoology
3 years completed

1989 - 1991 Bachelor of Science University of Guelph
Program in Biology
Graduated with Honours

1992 - 1993 Master of Science University of Toronto
Molecular and Medical Genetics
2 years completed; reclassified into Ph.D. program
Supervisor: Dr. Roderick R. McInnes

1994 - 2000 Doctor of Philosophy University of Toronto
Molecular and Medical Genetics
Supervisor: Dr. Roderick R. McInnes

Thesis Title: The role of Rom-1 in maintaining photoreceptor structure and viability, and a mathematical model exploring the kinetics of neuronal degeneration.

Geoffrey A. Clarke, Ph.D.

Professional Experience

2005 - Present Postdoctoral Fellow University of Toronto
Computational Biology
Supervisor: Dr. Charles J. Lumsden

2004 - 2005 Postdoctoral Fellow University of Toronto
Computational and Molecular Biology of the Insulin Response Network
Supervisor: Dr. Maria Rozakis-Adcock

2000 - 2004 Postdoctoral Fellow University of Toronto
Computational Biology
Supervisor: Dr. Charles J. Lumsden

1993 - 1998 Laboratory Manager Hospital for Sick Children, Toronto
Supervisor: Dr. Roderick R. McInnes

Summer 1991 Summer Research Student Hospital for Sick Children, Toronto
Supervisor: Dr. Roderick R. McInnes

Awards and Scholarships

Canadian Institutes for Health Research Postdoctoral Fellowship
2000 - 2003

Canadian Retinitis Pigmentosa Foundation Scholarship
1996 - 1998

University of Toronto Open Doctoral Fellowship
1997

Student Award Finalist (Predoctoral Basic category)
Annual Meeting of the American Society of Human Genetics,
San Francisco, 1996
For research on the photoreceptor-specific gene *ROM1*

Publications

Refereed Papers, Published:

Taylor, R.G., Grieco, D., **Clarke, G.A.**, McInnes, R.R., and Taylor, B.A. (1993). Identification of the mutation in murine histidinemia (*his*) and genetic mapping of the murine histidase locus (*Hal*) on chromosome 10. *Genomics* **16**:231-240.

Clarke, G., Héon, E. and McInnes, R.R. (2000). Recent advances in the molecular basis of inherited retinal dystrophies. *Clin. Genet.* **57**:313-329.

93 Wiley Ave, Toronto, On., M4J 3W5 (416) 778-6972 geoff.clarke@utoronto.ca

Refereed Papers, Published (continued):

Clarke, G., Goldberg, A.F.X., Vidgen, D., Collins, L., Ploder, L., Schwarz, L., Molday, L.L., Rossant, J., Szél, Á., Molday, R.S., Birch, D.G., and McInnes, R.R. (2000). Rom-1 is required for rod photoreceptor viability and the regulation of disk morphogenesis. *Nature Genet.* **25**:67-73.
Also see: Wright, A.F. (2000). For want of a disk the cell was lost. *Nature Med.* **6**: 508-509.

Clarke, G., Collins, R.A., Leavitt, B.R., Andrews, D.F., Hayden, M.R., Lumsden, C.J., and McInnes, R.R. (2000) A one-hit model of cell death in inherited neuronal degenerations. *Nature* **406**:195-199.
Also see: Heintz, N. One hit neuronal death. *Nature* **406**:137-138.

Clarke, G., Collins, R.A., Leavitt, B.R., Andrews, D.F., Hayden, M.R., Lumsden, C.J., and McInnes, R.R. (2001). Addendum: A one-hit model of cell death in inherited neuronal degenerations. *Nature* **409**:542.

Clarke, G., Lumsden, C.J., and McInnes, R.R. (2001). Inherited neurodegenerative diseases: the one-hit model of neurodegeneration. *Hum. Mol. Gen*. 10:2269-2275.

Kedzierski, W., Nusinowitz, S., Birch, D., **Clarke, G**., McInnes, R.R., Bok, D, and Travis, G.H. (2001). Deficiency of rds/peripherin causes photoreceptor death in mouse models of digenic and dominant retinitis pigmentosa. *Proc. Natl. Acad. Sci. USA* **98**:7718-7723.

Burns, J., **Clarke, G**., and Lumsden, C.J. (2002). Photoreceptor death: spatiotemporal patterns arising from one-hit death kinetics and a diffusible cell death factor. *Bull. Math. Biol*. **64**:1117-1145.

Clarke, G. and Lumsden, C.J. (2005). Heterogeneous cellular environments modulate one-hit neuronal death kinetics. *Bull. Brain Res*. **65**:59-67.

Clarke, G. and Lumsden C.J. (2005). Scale-free neurodegeneration: cellular heterogeneity and the stretched exponential kinetics of cell death. *J. Theor. Biol*. **233**:515-525.

Abstracts/ Presentations:

Taylor, R.G., Grieco, D., **Clarke, G.A.**, McInnes, R.R., and Taylor, B.A. (1992). Identification of the mutation in murine histidinemia (*his*), and linkage analysis of the mouse histidase gene (*Hal*) and the murine histidase activity variant (*Hsd*). *Am. J. Hum. Genet.* **51** (4, Supplement):A356

Clarke, G., Novak, J., Liu, I., Bascom, R., Ploder, L., and McInnes, R.R. Gene targeting to examine the roles of Chx10 and Rom1 in vertebrate central nervous system and retina development. Canadian Network Centers of Excellence Genetic Disease Network, Annual Meeting, 1993.

Abstracts/ Presentations (continued):

Clarke, G.., Stevenson, L., Rossant, J., and McInnes, R.R. Gene targeting of *Rom1*: generating mouse models of human degenerative retinopathies. University of Toronto, Department of Molecular and Medical Genetics, Annual Retreat, 1995.

Clarke, G., Stevenson, L., Rossant, J., and McInnes, R.R. Rom1 is required for the maintenance of normal photoreceptor structure. Great Lakes Mammalian Development Meeting, 1996.

Clarke, G., Stevenson, L., Rossant, J., and McInnes, R.R. Rom1 is required for the maintenance of normal photoreceptor structure. Canadian Network Centers of Excellence Genetic Disease Network, Annual Meeting, 1996.

Clarke, G., Kedzierski, W.,Rossant, J., Travis, G.H., and McInnes, R.R. (1996). Genetics of *ROM1*: evaluation of the requirement for rom-1 in photoreceptor morphogenesis and of the digenic hypothesis of retinitis pigmentosa. *Am. J. Hum. Genet.* **59** (4, Supplement):41

Birch, D.G., Locke, K., **Clarke, G.**, McInnes, R.R., and Travis, G.H. (1997). ERGs in mice with *Rds/Peripherin* and *Rom1* mutations. *Invest. Ophthalmol. Vis. Sci.* **38** (4):S316.

Travis, G.H., Kedzierski, W., **Clarke, G**., Birch, D., McInnes, R.R., and Bok, D. (1997) Digenic inheritance of photoreceptor degeneration in mice with mutations in the genes for both *Rds* and *Rom1*. *Invest. Ophthalmol. Vis. Sci.* **38** (4):S700.

Molday, L.L., Goldberg, A.F.X., **Clarke, G.**, McInnes, R.R. and Molday, R.S. Peripherin/rds assembles into a homotetramer which promotes rod and cone outer segment formation in rom-1 knockout mice: evidence for the subunit assembly model of digenic autosomal dominant retinitis pigmentosa. FASEB Biology and Chemistry of Vision Meeting at Keystone, Colorado, 1997.

Clarke, G., Rossant, J., and McInnes, R.R. (1998). Rom-1 is required for outer segment morphogenesis and photoreceptor viability. *Invest. Ophthalmol. Vis. Sci.* **39** (4):S962

Clarke, G., Collins, R.A., Lumsden, C.J., and McInnes, R.R. (1999). Why cells die in inherited neuronal degenerations (INDs): exponential death kinetics exclude cumulative damage, identify a constant or decreasing death risk, and suggest a mutant steady state model. *Am. J. Hum. Genet.* **65** (4, Supplement):A233.

Abstracts/ Presentations (continued):

Clarke, G. and Lumsden, C.J. Bistability and the commitment to cell death: a stochastic model of the mutant steady state. SIAM Symposium on Computational Models and Simulation for Intra-cellular Processes. Washington D.C., 2002

Clarke, G. and Lumsden, C.J.. A Stochastic Model of the Mutant Steady State (MSS): Bistability and the Commitment to Apoptotic Cell Death. American Society for Cell Biology, 42nd Annual Meeting, San Francisco, 2002

Invited Presentations:

December, 1994:
Molecular Genetics of Development.
Dentistry Graduate course in Medical Genetics, University of Toronto, School of Dentistry.
November, 1996:
Genetics of *ROM1*: Evaluation of the Requirement for Rom-1 in Photoreceptor Morphogenesis and of the Digenic Hypothesis of Retinitis Pigmentosa.
Presented to the American Society of Human Genetics
46th Annual Meeting, San Francisco.
Finalist: Student Award (Predoctoral Basic category) for research on the photoreceptor-specific gene ROM1.
February, 1997:
The Role of Rom1 in the Maintenance of Mammalian Photoreceptor Structure.
The Cleveland Clinic.

September, 2005:
Analysis of Complex Diseases: Experimental and Computational Approaches to Understanding Neurodegeneration and Diabetes.
University of Calgary, Department of Biology and Institute for Biocomplexity and Informatics

References:

Dr. Roderick R. McInnes, M.D., Ph.D.
Senior Scientist, The Hospital for Sick Children
Program in Genetic and Genomic Biology,
University Professor, University of Toronto.
Depts. of Molecular and Medical Genetics, Paediatrics,
CIHR Scientific Director, Institute of Genetics
Hospital for Sick Children
TMDT Building
101 College St.
Rm. 15-306, East Tower
Toronto, On
M5G 1X8
Phone: 416-813-6353
Fax: 416-813-4931
mcinnes@sickkids.ca

Dr. Charles J Lumsden, Ph.D.
Professor, University of Toronto
Institute of Medical Sciences
Clinical Sciences Division
Medical Sciences Building, Room 7313
1 King's College Circle
Toronto, On
M5S 1A8
Phone: 416-978-7178
Fax: 416-978-7171
charles.lumsden@utoronto.ca

Dr. Maria Rozakis-Adcock
Associate Professor
University of Toronto
Medical Sciences Building, Room 6238
1 King's College Circle
Toronto, On
M5S 1A8
Phone: 416-946-0392
Fax: 416-978-5959
maria.rozakis@utoronto.ca

Dr Derek van der Kooy
Professor, University of Toronto
Departments of Medical Genetics and Microbiology
Medical Sciences Building, Rm. 1105
1 King's College Circle
Toronto, Ontario
M5S 1A8
(416) 978-1960
derek.van.der.kooy@utoronto.ca

not elicit any Ca^{2+} response (data not shown). To measure MAP kinase activation, pEF6–*mil*, pEF6–*mil*^{m93} or pEF6–*mil*^{te273} were transiently co-tranfected with a reporter activated by MAP kinase-stimulated Elk-1 (Stratagene) into Jurkat T cells. Normalization of transfection was performed with a pCMV-Renilla luciferase construct and the Stop&Glo reagent (Promega). After stimulation with 100 nM S1P for 4 h, activities of the Firefly and Renilla luciferases were measured in cell lysates. The C305 anti-T-cell receptor antibody gave similar Ca^{2+} and MAP kinase responses in all transfectants.

Phenotypic rescue and genotyping

For RNA injections, the *mil* construct was generated by PCR using wild-type cDNA and cloned into pCS2+. Injected embryos were genotyped using allele-specific restriction fragment length polymorphisms.

Received 17 March; accepted 16 May 2000.

1. Chen, J. N. *et al.* Mutations affecting the cardiovascular system and other internal organs in zebrafish. *Development* **123,** 293–302 (1996).
2. Stainier, D. Y. R. *et al*. Mutations affecting the formation and function of the cardiovascular system in the zebrafish embryo. *Development* **123,** 285–92 (1996).
3. Yelon, D. *et al*. The bHLH transcription factor Hand2 plays parallel roles in zebrafish heart and pectoral fin development. *Development* **127,** 2573–2582 (2000).
4. Yelon, D., Horne, S. & Stainier, D. Y. R. Restricted expression of cardiac myosin genes reveals regulated aspects of heart tube assembly in zebrafish. *Dev. Biol.* **214,** 23–37 (1999).
5. Kikuchi, Y. *et al*. The zebrafish *bonnie and clyde* gene encodes a Mix family homeodomain protein that regulates the generation of endodermal precursors. *Genes Dev.* **14,** 1279–1289 (2000).
6. Reiter, J. F. *et al.* Gata5 is required for the development of the heart and endoderm in zebrafish. *Genes Dev.* **13,** 2983–2995 (1999).
7. Schier, A. F., Neuhauss, S. C., Helde, K. A., Talbot, W. S. & Driever, W. The *one-eyed pinhead* gene functions in mesoderm and endoderm formation in zebrafish and interacts with *no tail*. *Development* **124,** 327–342 (1997).
8. Alexander, J., Rothenberg, M., Henry, G. L. & Stainier, D. Y. R. *casanova* plays an early and essential role in endoderm formation in zebrafish. *Dev. Biol.* **215,** 343–357 (1999).
9. Alexander, J. & Stainier, D. Y. R. *Mutations affecting cardiac development in zebrafish* (eds. Harvey, R. & Rosenthal, N.) (Academic, San Diego, 1999).
10. Strähle, U., Blader, P., Henrique, D. & Ingham, P. W. *axial*, a zebrafish gene expressed along the developing body axis, shows altered expression in *cyclops* mutant embryos. *Genes Dev.* **7,** 1436–1446 (1993).
11. Knapik, E. W. *et al.* A microsatellite genetic linkage map for zebrafish (Danio rerio). *Nature Genet.* **18,** 338–343 (1998).
12. Chan, F. Y. *et al.* Characterization of adult alpha- and beta-globin genes in the zebrafish. *Blood* **89,** 688–700 (1997).
13. Martin, C. C., Laforest, L., Akimenko, M. A. & Ekker, M. A role for DNA methylation in gastrulation and somite patterning. *Dev. Biol.* **206,** 189–205 (1999).
14. Okazaki, H. *et al.* Molecular cloning of a novel putative G protein-coupled receptor expressed in the cardiovascular system. *Biochem. Biophys. Res. Commun.* **190,** 1104–1109 (1993).
15. An, S. *et al.* Identification of cDNAs encoding two G protein-coupled receptors for lysosphingolipids. *FEBS Lett.* **417,** 279–282 (1997).
16. MacLennan, A. J., Browe, C. S., Gaskin, A. A., Lado, D. C. & Shaw, G. Cloning and characterization of a putative G-protein coupled receptor potentially involved in development. *Mol. Cell. Neurosci.* **5,** 201–209 (1994).
17. An, S., Bleu, T. & Zheng, Y. Transduction of intracellular calcium signals through G protein-mediated activation of phospholipase C by recombinant sphingosine 1-phosphate receptors. *Mol. Pharmacol.* **55,** 787–794 (1999).
18. Goetzl, E. J. & An, S. Diversity of cellular receptors and functions for the lysophospholipid growth factors lysophosphatidic acid and sphingosine 1-phosphate. *FASEB J.* **12,** 1589–1598 (1998).
19. An, S., Zheng, Y. & Bleu, T. Sphingosine 1-phosphate-induced cell proliferation, survival, and related signaling events mediated by G protein-coupled receptors Edg3 and Edg5. *J. Biol. Chem.* **275,** 288–296 (2000).
20. Lee, M. J. *et al.* Sphingosine-1-phosphate as a ligand for the G protein-coupled receptor EDG-1. *Science* **279,** 1552–1555 (1998).
21. Forbes, A. & Lehmann, R. Cell migration in *Drosophila*. *Curr. Opin. Genet. Dev.* **9,** 473–478 (1999).
22. Zhang, N., Zhang, J., Purcell, K. J., Cheng, Y. & Howard, K. The *Drosophila* protein Wunen repels migrating germ cells. *Nature* **385,** 64–67 (1997).
23. Roberts, R., Sciorra, V. A. & Morris, A. J. Human type 2 phosphatidic acid phosphohydrolases. Substrate specificity of the type 2a, 2b, and 2c enzymes and cell surface activity of the 2a isoform. *J. Biol. Chem.* **273,** 22059–22067 (1998).
24. Scheer, A. *et al.* Mutational analysis of the highly conserved arginine within the glu/asp-arg-tyr motif of the α_{1b}-adrenergic receptor: effects on receptor isomerization and activation. *Mol. Pharmacol.* **57,** 219—231 (2000).
25. Strader, C. D., Fong, T. M., Tota, M. R., Underwood, D. & Dixon, R. A. Structure and function of G protein-coupled receptors. *Annu. Rev. Biochem.* **63,** 101–132 (1994).
26. Hla, T. *et al.* Sphingosine-1-phosphate: extracellular mediator or intracellular second messenger? *Biochem. Pharmacol.* **58,** 201–207 (1999).
27. Spiegel, S. Sphingosine 1-phosphate: a prototype of a new class of second messengers. *J. Leukocyte Biol.* **65,** 341–344 (1999).
28. Moolenaar, W. H. Bioactive lysophospholipids and their G protein-coupled receptors. *Exp. Cell Res.* **253,** 230–238 (1999).

Supplementary information is available on *Nature*'s World-Wide Web site (http://www.nature.com) or as paper copy from the London editorial office of *Nature*.

Acknowledgements

We thank I. Herskowitz, H. Bourne, C. Bargmann, R. Lehmann and members of the lab for discussions and comments on the manuscript. We are also grateful to A. Navarro for excellent fish care. E.K. is supported by the University of California President's post-doctoral fellowship program. This work was supported in part by the Program in Human Genetics Genomics Core Facility at UCSF as well as by grants to D.Y.R.S. from the American Heart Association and the Packard Foundation.

Correspondence and requests for materials should be addressed to D.Y.R.S. (e-mail: didier_stainier@biochem.ucsf.edu). The cDNA sequence of *mil* has been deposited in GenBank under accession number AF260256.

A one-hit model of cell death in inherited neuronal degenerations

Geoff Clarke*†, Richard A. Collins†, Blair R. Leavitt‡, David F. Andrews§, Michael R. Hayden‡, Charles J. Lumsden‖ & Roderick R. McInnes*†‖¶

** Programs in Developmental Biology and Genetics, The Research Institute, Hospital for Sick Children, 555 University Ave., Toronto, Ontario M5G 1X8, Canada*

† Departments of Molecular and Medical Genetics, ¶ Pediatrics, and ‖ Department of Medicine, Institute of Medical Science, University of Toronto, 1 King's College Circle, Toronto, Ontario M5S 1A8, Canada

‡ Centre for Molecular Medicine and Therapeutics, Department of Medical Genetics University of British Columbia, Vancouver, British Columbia V5Z 4H4, Canada

§ Department of Statistics, University of Toronto, 100 St. George Street, M5S 3G3, Canada

In genetic disorders associated with premature neuronal death, symptoms may not appear for years or decades. This delay in clinical onset is often assumed to reflect the occurrence of age-dependent cumulative damage[1–6]. For example, it has been suggested that oxidative stress disrupts metabolism in neurological degenerative disorders by the cumulative damage of essential macromolecules[1,4,7]. A prediction of the cumulative damage hypothesis is that the probability of cell death will increase over time. Here we show in contrast that the kinetics of neuronal death in 12 models of photoreceptor degeneration, hippocampal neurons undergoing excitotoxic cell death[8], a mouse model of cerebellar degeneration[9] and Parkinson's[10] and Huntington's diseases are all exponential and better explained by mathematical models in which the risk of cell death remains constant or decreases exponentially with age. These kinetics argue against the cumulative damage hypothesis; instead, the time of death of any neuron is random. Our findings are most simply accommodated by a 'one-hit' biochemical model in which mutation imposes a mutant steady state on the neuron and a single event randomly initiates cell death. This model appears to be common to many forms of neurodegeneration and has implications for therapeutic strategies.

To distinguish between the increasing risk of death associated with cumulative damage (which would generate a sigmoidal decline in cell number) and the exponential decline in cell number that results from a constant or decreasing risk of death (Fig. 1a), we used regression analysis to analyse photoreceptor neuron death in 11 animal models of inherited retinal degeneration and an experimental model of retinal detachment. These models include animals with mutations in genes encoding a range of proteins including the photosensitive pigment rhodopsin (M. M. LaVail, personal communication), the enzyme cyclic GMP phosphodiesterase[11,12] and the structural proteins rom-1 (ref. 13) and peripherin/rds[14,15]. In three other mutants analysed, the affected gene is unknown.

In five of these examples (Fig. 1, Table 1, and see Supplementary Information), the data fit only to mathematical models in which the probability of photoreceptor death remains constant with age. In six

others (Fig. 2, Table 1), the kinetics fit equally well to models of constant or exponentially decreasing risk of death. Consequently, in all of these animal models the increasing risk of photoreceptor death predicted by the cumulative damage hypothesis can be excluded, a possible exception being the $Rd^{-/-}$ mouse in which the data (Fig. 1d) fit equally well to models of constant ($R^2 = 0.985$, $P < 0.001$) and exponentially increasing risk ($R^2 = 0.980$; $P < 0.001$). Thus, even if age-dependent cumulative damage does occur in these mutant retinas, it is not associated with an increase in the probability that the photoreceptors will die.

In agreement with these direct measurements of the kinetics of photoreceptor death in animal models, clinical assessment of photoreceptor function in patients with retinitis pigmentosa and cone-rod dystrophy has shown that both visual field loss[16] and the decay of the maximum photoreceptor electroretinogram responses also observe exponential kinetics[17,18]. Thus, the exponential cell death kinetics that we have identified in animal models appear to be shared by most, if not all, examples of inherited retinal degeneration.

To determine whether a constant or exponentially decreasing risk of neuronal death is a general phenomenon shared by other classes of neuron, we examined the kinetics of neurodegeneration in four other diseases or experimental models. Neuronal loss in the substantia nigra in Parkinson's disease[10], the excitotoxic death of cultured hippocampal neurons[8] and the loss of cerebellar granule cells in *pcd/pcd* (Purkinje cell degeneration) mice[9] have been shown to produce an exponential decline in neuronal number with time. Our regression analyses demonstrate that only a constant risk describes the kinetics of cell death in the first two of these examples (Table 1, Fig. 3a, b). On the other hand, the loss of cerebellar granule cells subsequent to the genetically determined loss of their target Purkinje neurons in *pcd/pcd* mice[9] (Fig. 3c) and neuronal death in a

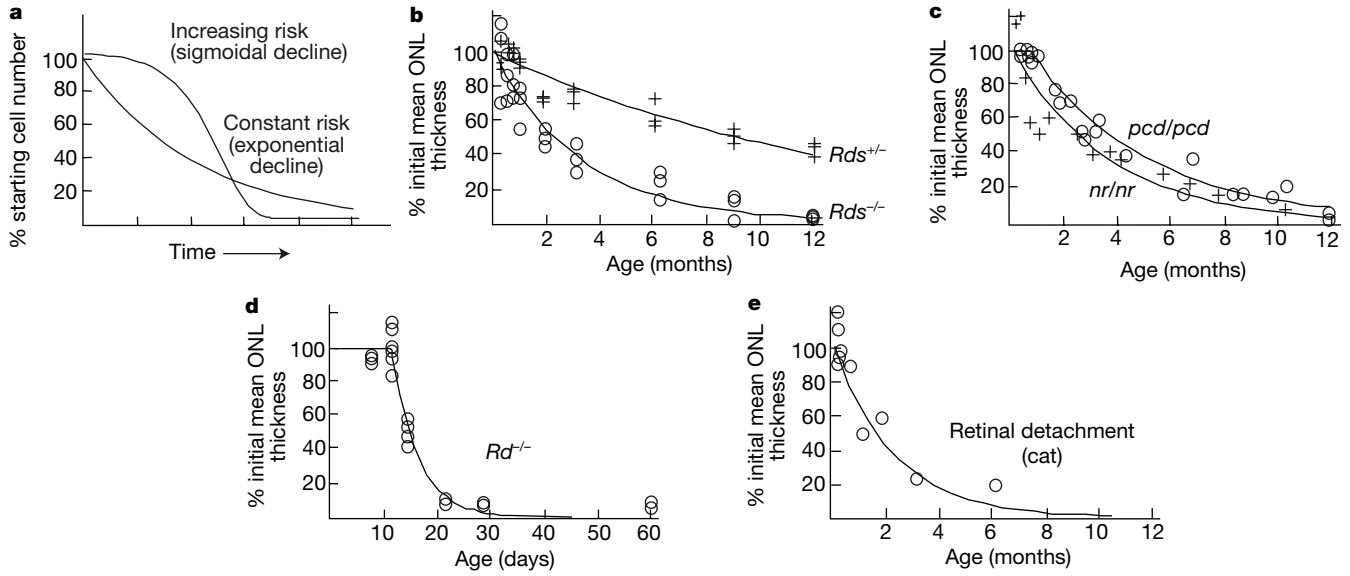

Figure 1 Animal models of inherited photoreceptor degeneration and retinal detachment, in which the kinetics of cell death are best described by a constant risk of neuronal death (see equations (1) and (3) in Methods). **a**, Constant and increasing risk of neuronal death will manifest as an exponential or sigmoidal decline in cell number, respectively. **b**, *Retinal degeneration slow* heterozygous ($Rds^{+/-}$)[15] and homozygous mice ($Rds^{-/-}$)[15] carrying a null mutation in the gene encoding peripherin/rds. **c**, *Nervous* homozygous mice (*nr/nr*)[27], and *purkinje cell degeneration* mice (*pcd/pcd*)[28]. **d**, Mice homozygous for a null mutation in the gene encoding the phototransduction enzyme rod cGMP β-phosphodiesterase ($Rd^{-/-}$)[14]. **e**, Experimental retinal detachment in the cat[24].

Table 1 Parameter estimates for kinetic models relating the risk of neuronal death (μ) to age

Animal model	Constant μ: $\frac{d\mathrm{ONL}(t)}{dt} = -\mu \times \mathrm{ONL}(t)$			Exponentially decreasing μ: $\frac{d\mathrm{ONL}(t)}{dt} = -\mu_0 e^{-At} \times \mathrm{ONL}(t)$			
	μ	ONL(0)	R^{2*}	μ_0	A	ONL(0)	R^{2*}
$Rds^{+/-}$ mice[15]	0.0170	49.4 μm	0.992	N/A	N/A	N/A	rejected†
$Rds^{-/-}$ mice[15]	0.0729	40.5 μm	0.968	N/A	N/A	N/A	rejected†
nr/nr mice‡[27]	0.278	50.1 μm	0.953	N/A	N/A	N/A	rejected†
Photoreceptors of *pcd/pcd* mice[28]	0.223	10.6 nuclei	0.992	N/A	N/A	N/A	rejected†
Retinal detachment (cat)‡[24]	0.00752	220 nuclei per mm	0.976	N/A	N/A	N/A	rejected†
$Rom1^{-/-}$ mice[13]	0.0316	37.7 μm	0.993	0.0666	0.103	41.9 μm	0.995
pd (miniature schnauzer)[12]	2.24	12.1 nuclei	0.979	3.13	1.12	13.1 nuclei	0.992
Albino (Balb/cHeA) mice[14]	0.00917	51.7 μm	0.995	0.0235	0.0485	51.7 μm	0.997
rcd-1 (Irish setter)[11,12]	0.0289	10.6 nuclei	0.957	0.0483	0.086	11.8 nuclei	0.970
$Rd^{-/-}$;$Rds^{-/-}$ mice[14]	0.123	45.4 μm	0.992	0.208	0.0912	45.3 μm	0.996
P23H rhodopsin-expressing transgenic rat§	0.0095	46.8 μm	0.975	0.0172	0.00752	55.0 μm	0.987
$Rd^{-/-}$ mice[14]	0.208	42.2 μm	0.985	N/A	N/A	N/A	rejected†
Cultured hippocampal neurons[8]	0.0773	100% of normal	0.996	N/A	N/A	N/A	rejected†
Parkinson's disease[10]	0.0858	100% of normal	0.919	N/A	N/A	N/A	rejected†
Granule cell degeneration in *pcd/pcd* mice[9]	0.006	5,999.52 cells	0.990	0.0076	0.0018	6,000 cells	0.990
Chemically-induced rat model of Parkinson's disease[19]‡	0.207	100% of normal	0.967	0.537	0.310	100%	0.999

* R^2 values reflect the proportion of data variability that is explained by the model. All reported R^2 values were statistically significant ($P < 0.001$).
† Parameter estimates were not significantly different from zero.
‡ Regressions performed on mean values reported in literature.
N/A, not applicable.
§ M. M. LaVail, personal communication.

chemically induced rat model of Parkinson's disease[19] (Fig. 3d) can both be described by either a constant or an exponentially decreasing risk of cell death (Table 1). We also measured ^{18}F-doxyglucose uptake in the caudate nuclei of patients with Huntington's disease as an indirect measure of neuronal loss. Because each of these patients was repeatedly tested at various times after clinical onset, the glucose uptake data, predictably, is highly variable in the whole population of patients (see Supplementary Information). Consequently, analysis of neuronal degeneration kinetics in this heterogeneous population necessitated the use of repeated-measures regression for each individual (see Methods). We found that neurodegeneration in these patients is also best described by a constant risk of cell death (Fig. 3e). Thus, our identification of similar cell death kinetics in five different types of neuron indicates that a constant or decreasing risk of cell death may be common to many forms of neurodegeneration. Although neuronal death is mediated by apoptosis in all photoreceptor degenerations examined (for example, refs 7, 20), it remains to be determined whether a constant or exponentially decreasing risk of death will be found invariably to accompany neuronal apoptosis.

Although the available data do not allow us to distinguish conclusively between constant and exponentially decreasing risk, both models indicate that the time of death of an individual neuron is random. Nevertheless, the two models have quite different pathophysiological implications. In a process involving constant risk, the time of death of an individual neuron is not only random, but also independent of the time of death of any other neuron. In this case, the kinetics of neuronal degeneration are comparable to the simple exponential decay exhibited by radioactive compounds, and the different rates of photoreceptor degeneration (Fig. 1) are determined largely or solely by the mutant genotype. In contrast, exponentially decreasing risk indicates that the chance of cell death decreases in direct proportion to the number of remaining cells. Such kinetics could result from an increase in the concentration of a

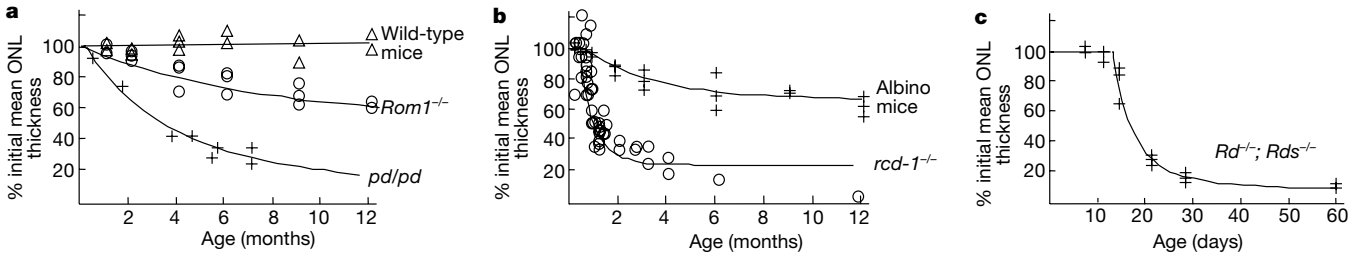

Figure 2 Animal models of inherited photoreceptor degeneration in which the kinetics of cell death are best described by an exponentially decreasing risk of death (see equations 1 and 2 in Methods). **a**, Wild-type and *Rom1*$^{-/-}$ mice[13], and photoreceptor dysplasia (*pd/pd*) in miniature schnauzers[12]. **b**, Albino mice[14] (Balb/cHeA) and rod-cell degeneration (*rcd-1*) in Irish setters[11,12] due to a null mutation in the rod cGMP β-phosphodiesterase gene. **c**, Mice homozygous for null mutations in both the gene encoding rod cGMP β-phosphodiesterase and the gene encoding peripherin/rds (*Rd*$^{-/-}$;*Rds*$^{-/-}$)[14].

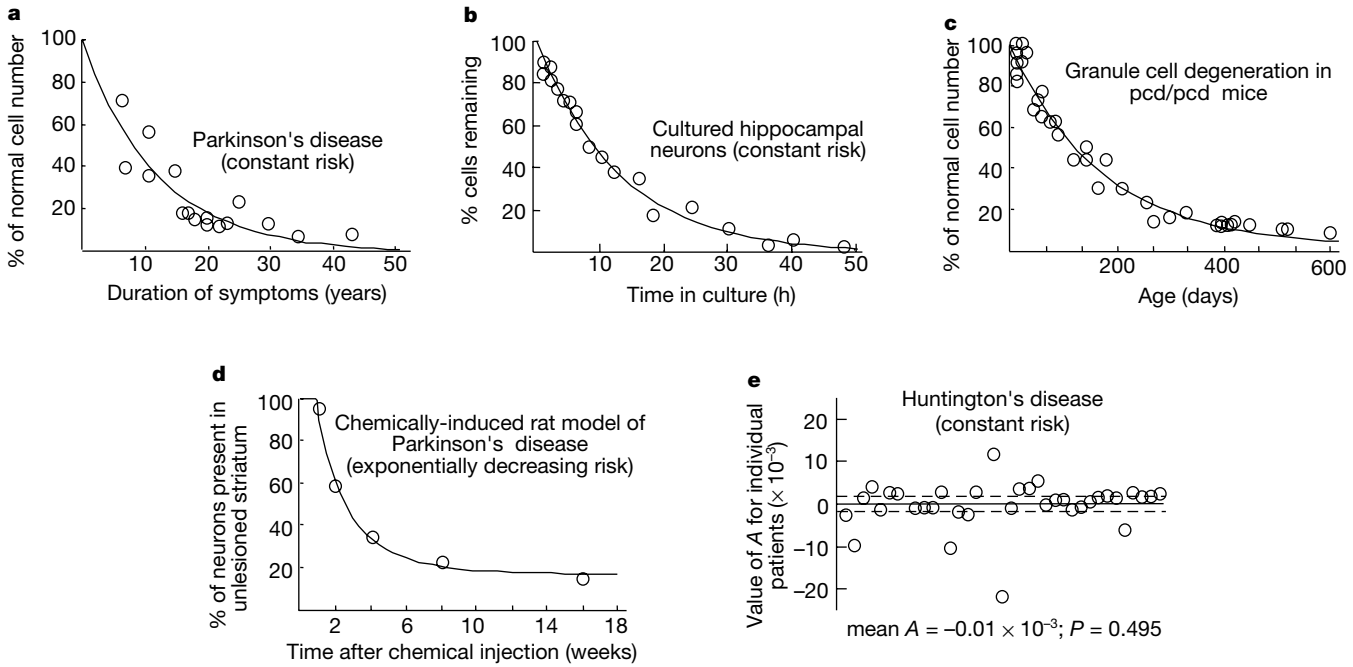

Figure 3 Examples of non-retinal neuronal death that display a constant or exponentially decreasing risk of death. **a**, The number of neurons (% of normal) in the substantia nigra of patients with Parkinson's disease as a function of symptom duration[10] is best described by a constant probability of neuronal death. **b**, Cultured hippocampal neurons undergoing excitotoxic cell death after incubation with glutamate exhibit a constant risk of cell death[8]. **c**, In contrast, the secondary loss of cerebellar granule cells[9] is described equally well by either a constant or an exponentially decreasing risk of cell death; the curve represents a constant risk. **d**, The percentage of substantia nigra neurons present in rats after injection with the neurotoxin 6-hydroxydopamine[19], a chemically induced animal model of Parkinson's disease, is best fit by an exponentially decreasing risk of neuronal death. **e**, The kinetics of metabolic decline in Huntington's disease patients are best fit by a constant risk of cell loss. Values of A (in the exponent of equation (5), see Methods) do not differ significantly from zero (P = 0.495, Student's t-test). Each point represents the estimated A for an individual patient. Solid line, mean A (mean ± s.d.: $-0.01 \times 10^{-3} \pm 5.3 \times 10^{-3}$ mM h^{-1}, n = 38 patients) across patient population; dashed lines, 95% confidence interval for the mean value of A (-1.7×10^{-3}, 1.7×10^{-3}).

survival factor, such as basic fibroblast growth factor or ciliary neurotrophic factor[21], or from a decrease in the amount of a toxic factor as the population of cells declines. Consistent with the latter possibility, dying retinal progenitor cells have been shown to produce an apoptosis-inducing agent[22].

An alternative interpretation for the exponential decline in risk is that the decrease is an artefact resulting from the presence of two neuronal populations, each with different but constant risks of cell death. For photoreceptor degenerations, this possibility is excluded by the fact that 97% of mouse photoreceptors are rods and only 3% are cones[23]. This proportion of cones is too small to influence the overall kinetics of photoreceptor death. Furthermore, the data for all six models exhibiting a decreasing risk do not fit a simple equation incorporating two exponential functions (see Supplementary Information), which also suggests that the presence of two differentially affected cell populations is not responsible for the exponentially decreasing risk of cell death.

Any model of the mechanisms underlying inherited neuronal degenerations must account for the major features of cell death in these disorders. These features are (1) the constant or decreasing risk of neuronal death described above; (2) the genotype-dependent nature of the risk; (3) the random time of death of any cell (illustrated by the random distribution of apoptotic photoreceptors seen in the retinas of animals and humans with inherited retinal degenerations[13,20]); and (4) the paradoxical situation in which most neurons in animals or patients with inherited neurodegenerations survive and function normally for months, years or decades, while a few genetically identical cells in the population are dying randomly.

We propose that these features can be explained if the mutant neurons are in an abnormal homeostatic state, the mutant steady state (MSS). The MSS differs little from the normal neuronal steady state (as most of the mutant cells are alive and functioning normally), except that the MSS is associated with an increased risk of cell death. We suggest that the MSS is a response to mutation characterized by subtle but critical changes in the expression or function of relatively few 'mutant response' genes or proteins (MuRGs or MuRPs, respectively), which mediate critical pre-death reactions. If MuRP is an enzyme, for example, it may change the relative concentrations of 'pre-lethal' molecules (Fig. 4). Exit from the MSS and commitment to cell death would occur when random fluctuations in the concentrations of pre-lethal molecules exceed a threshold beyond which neuronal death is initiated. Different mutations would shift the steady state to varying degrees, so that mutations producing a transition to an MSS closer to the cell-death threshold have a greater chance of exceeding that threshold, and therefore a higher probability of causing cell death. Thus, we propose a 'one-hit' model in which the death of an individual neuron is initiated randomly in time by a single rare catastrophic event.

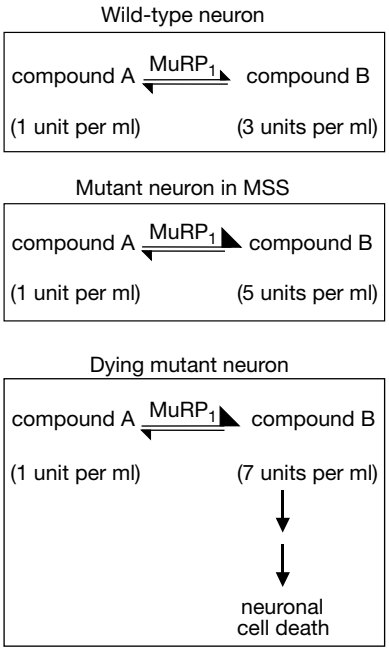

Figure 4 The exponential kinetics of cell death in inherited neuronal degenerations suggest the existence of a mutant steady state (MSS) in which the risk of cell death is increased. In wild-type neurons, a reaction, catalysed for example by the enzyme $MuRP_1$, is associated with a concentration of compound B of 3 units per ml. In a mutant neuron in the MSS, the $MuRP_1$ activity changes in response to the mutation, so that the concentration of compound B is increased to 5 units per ml. Random increases in the concentration of compound B to 7 units per ml will trigger cell death.

A similar one-hit kinetic model has been proposed and rejected as an explanation for the exponential cell death kinetics exhibited by cultured hippocampal neurons exposed transiently to excitotoxic amino acids[8]. The one-hit model was rejected in favour of a more complex mechanism involving a multistep biochemical cascade in which the overall death rate is determined by the specific rate constants for each of an unknown number of transitions within the cascade. We suggest, however, that some environmental insults place neurons in an abnormal steady state which, like the MSS, is associated with a constant increased risk of death. This environmentally induced abnormal steady state is exemplified by the effect of excitotoxic amino acids in initiating the exponential death of hippocampal neurons[8] (Fig. 3b, Table 1) and by the effect of retinal detachment in leading to photoreceptor death[24] (Fig. 1e, Table 1).

Our findings have important implications for the understanding and treatment of retinal and possibly other types of neuronal degeneration. First, biochemical mechanisms proposed to underlie neuronal death must be re-examined in light of the constant or exponentially decreasing risk of cell death that we have identified. Second, identification of the MuRGs and MuRPs in different mutant neurons will indicate whether mutations impose MSSs that share common MuRGs and MuRPs, or whether each MSS is uniquely or partly defined by the specific mutant gene or mutation. In mutant neurons in which the risk of death is constant throughout life, the MSS should be the same in young and old cells with the same genotype, although additional secondary changes in gene or protein expression may occur as a consequence of cell death. Alternatively, in models in which the risk of death decreases exponentially, cell death may be associated with a changing pattern of MuRGs and MuRPs. In either case, identification of MuRGs and MuRPs in different mutants is likely to provide insight into the pathogenic events that increase the risk of cell death in the MSS. Pharmacological intervention to shift the activity of MuRGs and MuRPs towards normal levels should slow or prevent initiation of the biochemical cascade leading to cell death. Finally, the absence of cumulative damage means that the likelihood that a mutant neuron can be rescued by treatment is not diminished by age, although fewer cells will be available to rescue. Therefore, treatment at any stage of the illness is likely to confer benefit. □

Methods

Measurements and statistical analysis

We examined the kinetics of photoreceptor degeneration in animal models in which cell loss had been reported quantitatively over at least one year, or until most photoreceptors had died. The kinetics of cell loss were analysed by fitting either the outer nuclear layer (ONL) thickness or cell number data to solutions of the differential equation

$$\frac{d\mathrm{ONL}(t)}{dt} = -\mu(t) \times \mathrm{ONL}(t) \quad (1)$$

where $\mu(t)$ represents the risk of cell death at age t. Functions for $\mu(t)$ were substituted as

follows:

$$\text{exponentially decreasing risk} \quad \mu(t) = \mu_0 e^{-A(t-\text{delay})} \tag{2}$$

$$\text{constant risk} \quad \mu(t) = \mu_0 \tag{3}$$

$$\text{exponentially increasing risk} \quad \mu(t) = \mu_0 e^{A(t-\text{delay})} \tag{4}$$

where μ_0 represents the initial probability of cell death and delay represents the time before neuronal death begins. Equations for $\mu(t)$ were chosen on the basis of their ability to yield exponential and sigmoidal curves. Data fitting was performed using nonlinear regression analysis (quasi-Newton methods), a method of modelling the relationship between variables, using the functions in the Mathematica 3.0 (Wolfram Research) software package[25]. Models were rejected if parameter estimates did not differ significantly ($P < 0.05$) from zero.

Measurements of metabolic decline in the caudates of 38 patients with Huntington's disease were obtained from PET scans as described[26]. For each patient, average glucose uptake over the course of at least three years was fit to the solution of the differential equation:

$$\frac{d\text{ONL}(t)}{dt} = \mu e^{At} \times \text{ONL}(t) \tag{5}$$

to provide an estimate of A. $A > 0$ corresponds to increasing risk, $A < 0$ to decreasing risk, and $A = 0$ to constant risk. Estimates of A for each subject were then averaged, and a Student's t-test was used to determine whether the mean value was significantly different from zero ($P < 0.05$).

Received 15 February; accepted 22 May 2000.

1. Coyle, J. T. & Puttfarken, P. Oxidative stress, glutamate, and neurodegenerative disorders. *Science* **262,** 689–695 (1993).
2. Cummings, J. L., Vinters, H. V., Cole, G. M. & Khachaturian, Z. S. Alzheimer's disease: etiologies, pathophysiology, cognitive reserve, and treatment opportunities. *Neurology* **51,** S2–17 (1998).
3. Alves-Rodrigues, A., Gregori, L. & Figueiredo-Pereira, M. E. Ubiquitin, cellular inclusions and their role in neurodegeneration. *Trends Neurosci.* **21,** 516–520 (1998).
4. Cassarino, D. S. & Bennett, J. P. Jr An evaluation of the role of mitochondria in neurodegenerative diseases: mitochondrial mutations and oxidative pathology, protective nuclear responses, and cell death in neurodegeneration. *Brain Res. Rev.* **29,** 1–25 (1999).
5. Selkoe, D. J. Translating cell biology into therapeutic advances in Alzheimer's disease. *Nature* **399,** A23–A31 (1999).
6. Dunnett, S. B. & Björklund, A. Prospects for new restorative and neuroprotective treatments in Parkinson's disease. *Nature* **399,** A32–A39 (1999).
7. Travis, G. H. Mechanisms of cell death in the inherited retinal degenerations. *Am. J. Hum. Genet.* **62,** 503–508 (1998).
8. Dubinsky, J. M., Kristal, B. S. & Elizondo-Fournier, M. On the probabilisitic nature of excitotoxic neuronal death in hippocampal neurons. *Neuropharmacology* **34,** 701–711 (1995).
9. Triarhou, L. C. Rate of neuronal fallout in a transsynaptic cerebellar model. *Brain Res. Bull.* **47,** 219–222 (1998).
10. Fearnley, J. M. & Lees, A. J. Ageing and Parkinson's disease: substantia nigra regional selectivity. *Brain* **114,** 2283–2301 (1991).
11. Schmidt, S. Y. & Aguirre, G. D. Reductions in taurine secondary to photoreceptor loss in Irish setters with rod-cone dysplasia. *Invest. Ophthalmol. Vis. Sci.* **26,** 679–683 (1985).
12. Parshall, C. J., Wyman, M., Nitroy, S., Acland, G. & Aguirre, G. Photoreceptor dysplasia: an inherited progressive retinal atrophy of miniature schnauzer dogs. *Prog. Vet. Comp. Ophthalmol.* **1,** 187–203 (1991).
13. Clarke, G. *et al.* Rom-1 is required for rod photoreceptor viability and the regulation of disk morphogenesis. *Nature Genet.* **25,** 67–73 (2000).
14. Sanyal, S. & Hawkins, R. K. Genetic interaction in the retinal degeneration of mice. *Exp. Eye Res.* **33,** 213–222 (1981).
15. Hawkins, R. K., Jansen, H. G. & Sanyal, S. Development and degeneration of retina in *rds* mutant mice: photoreceptor abnormalities in the heterozygotes. *Exp. Eye Res.* **41,** 701–720 (1985).
16. Massof, R. W., Dagnelie, G., Benzschawel, T., Palmer, R. W. & Finkelstein, D. First order dynamics of visual field loss in retinitis pigmentosa. *Clin. Vis. Sci.* **5,** 1–26 (1990).
17. Berson, E. L., Sandberg, M. A., Rosner, B., Birch, D. G. & Hanson, A. H. Natural course of retinitis pigmentosa over a three-year interval. *Am. J. Ophthalmol.* **99,** 240–251 (1985).
18. Birch, D. G., Anderson, J. L. & Fish, G. E. Yearly rates of rod and cone functional loss in retinitis pigmentosa and cone-rod dystrophy. *Ophthalmology* **106,** 258–268 (1999).
19. Sauer, H. & Oertel, W. H. Progressive degeneration of nigrostriatal dopamine neurons following intrastriatal terminal lesions with 6-hydroxydopamine: a combined retrograde tracing and immunocytochemical study in the rat. *Neuroscience* **59,** 401–415 (1994).
20. Li, Z.-Y. & Milam, A. H. in *Degenerative Diseases of the Retina* (eds Anderson, R. E., LaVail, M. M. & Hollyfield, J. G.) 1–8 (Plennum, New York, 1995).
21. Wen, R. *et al.* Injury-induced upregulation of bFGF and CNTF mRNAs in the rat retina. *J. Neurosci.* **15,** 7377–7385 (1995).
22. Seigal, G. S. & Liu, L. Inducible, apoptosis-promoting activity in retinal cell-conditioned medium. *Mol. Vision* **3,** 14 (1997).
23. Carter-Dawson, L. D. & LaVail, M. M. Rods and cones in the mouse retina. I. Structural analysis using light and electron microscopy. *J. Comp. Neurol.* **188,** 245–262 (1979).
24. Erickson, P. A., Fisher, S. K., Anderson, D. H., Stern, W. H. & Borgula, G. A. Retinal detachment in the cat: the outer nuclear and outer plexiform layers. *Invest. Ophthalmol. Vis. Sci.* **24,** 927–942 (1983).
25. Ratkowsky, D. A. *Nonlinear Regression Modeling: A Unified Practical Approach* (Marcel Decker, New York, 1983).
26. Kremer, B. *et al.* Influence of lamotrigine on progression of early Huntington's disease: a randomized clinical trial. *Neurology* **53,** 1000–1011 (1999).
27. La Vail, M. M. *et al.* Retinal degeneration in the nervous mouse. I. Light microscopic cytopathology and changes in the interphotoreceptor matrix *J. Comp. Neurol.* **333,** 168–181 (1993).
28. LaVail, M. M., Blanks, J. C. & Mullen, R. J. Retinal degeneration in the pcd cerebellar mouse. I. Light microscopic and autoradiographic analysis. *J. Comp. Neurol.* **212,** 217–230 (1982).

Supplementary information is available on *Nature*'s World-Wide Web site (http://www.nature.com) or as paper copy from the London editorial office of *Nature*.

Acknowledgements

We thank the physicians of the Huntington's disease patients for their help and support of this study; M. LaVail for sharing unpublished data on P23H rhodopsin-expressing transgenic rats; and A. G. Kundson Jr, T. P. Dryja, D. J. Zack, H. Lipshitz, M. W. Salter and S. Meyn for critical reading of the manuscript. This work was supported by grants from the Foundation Fighting Blindness (R.R.M.), The Macular Vision Research Foundation (R.R.M.), The RP Eye Research Foundation of Canada (R.R.M.), MRC of Canada (M.R.H. and B.R.L.), the Canadian Genetic Disease Network (R.R.M. and M.R.H.) and the Huntington Disease Society of America (M.R.H.). M.R.H. is an Established Investigator of the BC Children's Hospital. R.R.M. is an International Research Scholar of the Howard Hughes Medical Institute.

Correspondence and requests for materials should be addressed to R.R.M. (e-mail: mcinnes@sickkids.on.ca).

Genetic ablation of parathyroid glands reveals another source of parathyroid hormone

Thomas Günther*†, Zhou-Feng Chen†‡, Jaesang Kim§, Matthias Priemel‖, Johannes M. Rueger‖, Michael Amling‖, Jane M. Moseley¶, T. John Martin¶, David J. Anderson§ & Gerard Karsenty*

** Department of Molecular and Human Genetics, Program of Developmental Biology, Baylor College of Medicine, 1 Baylor Plaza, Houston, Texas 77030, USA*
‡ Department of Anesthesiology, Washington University School of Medicine, 660 South Euclid Avenue, St. Louis, Missouri 63110, USA
§ Howard Hughes Medical Institute and Division of Biology, California Institute of Technology, Pasadena, California 91125, USA
‖ Department of Trauma Surgery, Hamburg University, Martinistrasse 52, 20246 Hamburg, Germany
¶ St. Vincent's Institute of Medical Research, 9 Princes Street, Fitzroy 3065, Melbourne, Victoria, Australia
† These authors contributed equally to this work

The parathyroid glands are the only known source of circulating parathyroid hormone (PTH), which initiates an endocrine cascade that regulates serum calcium concentration[1]. *Glial cells missing2* (*Gcm2*), a mouse homologue of *Drosophila Gcm*, is the only transcription factor whose expression is restricted to the parathyroid glands[2–5]. Here we show that *Gcm2*-deficient mice lack parathyroid glands and exhibit a biological hypoparathyroidism, identifying *Gcm2* as a master regulatory gene of parathyroid gland development. Unlike *PTH receptor*-deficient mice, however, *Gcm2*-deficient mice are viable and fertile, and have only a mildly abnormal bone phenotype. Despite their lack of parathyroid glands, *Gcm2*-deficient mice have PTH serum levels identical to those of wild-type mice, as do parathyroidectomized wild-type animals. Expression and ablation studies identified the thymus, where *Gcm1*, another Gcm homologue, is expressed, as the additional, downregulatable source of PTH. Thus, *Gcm2* deletion uncovers an auxiliary mechanism for the regulation of calcium homeostasis in the absence of parathyroid glands. We propose that this backup mechanism may be a general feature of endocrine regulation.

Serum calcium is essential for many physiological functions including muscle contraction, blood coagulation, neuromuscular excitability and mineralization of bone, a tissue that contains 99%

ELSEVIER

Brain Research Bulletin 65 (2005) 59–67

BRAIN RESEARCH BULLETIN

www.elsevier.com/locate/brainresbull

Heterogeneous cellular environments modulate one-hit neuronal death kinetics

Geoff Clarke, Charles J. Lumsden*

Department of Medicine, and Institute of Medical Science, University of Toronto, Medical Sciences Building, 1 King's College Circle, Room 7313, Toronto, Ont., Canada M5S 1A8

Received 16 January 2004; received in revised form 10 November 2004; accepted 11 November 2004
Available online 15 December 2004

Abstract

We recently demonstrated that cell loss kinetics in diverse forms of neurodegeneration (ND) suggests a universal death switch mechanism in which each cell is at a constant risk to initiate apoptosis. We proposed that mutant and injured neurons exist in a viable state typified by an increased risk of initiating death processes [Clarke, Collins, Leavitt, Andrews, Hayden, Lumsden, McInnes, A one-hit model of cell death in inherited neuronal degenerations, Nature 406 (2000) 195–199]. To date, however, measurements of cell death risk have been available only as averages across the affected cell population. Here we develop and apply a method of death kinetic analysis in which the risk factors vary across the neuronal population, as for example due to regional heterogeneities in the cellular microenvironment. We find that most cases of ND for which cell loss data has been obtained are better explained by death risks that vary from cell to cell, compared to death risk that is constant across the neuronal population. Strikingly, a common form of the frequency distribution defining the death risk heterogeneity is shared across most of these cases. This first characterization of the kinetic heterogeneity in one-hit neuronal death, therefore, suggests that the wide variety of ND now known may share mechanisms through which regional differences in the cellular microenvironment modulate the kinetics of cell loss.

Keywords: Neurodegeneration; Mutant steady state; Lifetime distribution

1. Introduction

Neurodegenerative disorders are a heterogeneous group of diseases that normally strike late in life, often with devastating consequences for the affected individuals and their families. Parkinson's disease, for example, results in a decline in physical abilities, manifesting as resting tremors, rigidity, a decrease in the rapidity and amplitude of movements, difficulty initiating new movements, and postural instability [18,41]. Disorders such as Huntington's disease inflict psychiatric disturbances and bring about increasing difficulties performing cognitive tasks [17,38]. The economic toll resulting from neurodegenerative diseases is remarkable. As of 1997 the direct and indirect costs associated with the treatment of patients with Alzheimer's disease were estimated to be on the order of $70 billion dollars (1991 currency) per year in the United States alone [3,13]. These burdens will increase as the North American population ages.

The characterization of the genetic and environmental factors that cause neurodegeneration (ND) has progressed significantly in recent years. This success is exemplified by the pace at which the genes responsible for inherited blindness have been identified. Approximately 150 genetic loci associated with diseases of the retina are known, and the genes for roughly 100 of them have been isolated (RetNet, http://www.sph.uth.tmc.edu/Retnet/, and [31]). Identification of such primary causes of ND, and the subsequent development of in vivo and in vitro methods designed to analyze the molecular mechanisms by which the disease symptoms

* Corresponding author. Tel.: +1 416 978 7178; fax: +1 416 978 3701.
E-mail address: charles.lumsden@utoronto.ca (C.J. Lumsden).

0361-9230/$ – see front matter © 2004 Elsevier Inc. All rights reserved.
doi:10.1016/j.brainresbull.2004.11.009

arise, indicate that the underlying neuronal attrition involves programmed cell death [40,41]. The mechanisms responsible for initiating the cell death process are, however, still poorly understood. For example, mutations that result in photoreceptor degeneration are found in genes encoding proteins that function as signal transduction molecules, transcription factors, and structural proteins [31]. This diversity of potential effectors has led to a range of proposals about the actual mechanisms of neuronal cell death initiation, including oxidative damage [25], accumulation of nuclear or cytoplasmic protein aggregates [20], or disruption of calcium homeostasis [24].

An important trait of ND is the kinetics by which cells are lost from the affected population: if normal function requires certain minimal numbers and configurations of neurons in specific pathways and circuits, then the ND kinetics establishes the time scales over which cell attrition eradicates the function and identifies the intervals during which loss is greatest. To date, this feature has received less attention than have biochemical and genomic characterization. Recently, we demonstrated that the kinetics of cell loss in many forms of both inherited and acquired neurodegeneration can be accurately described as a one-hit process in which the risk of cell death is constant [5]. To account for this observation we postulated the existence of an alternative cellular state, the mutant steady state (MSS), in which the affected cells are viable but have an increased risk of undergoing cell death compared to normal cells [5,6,31]. This risk of death to cells in the normal state is sufficiently low as to have no impact on the pattern of cell attrition over time. The simplest case for degenerating cell populations is that in which all cells in the MSS share the same risk value. Such population-wide uniformity of death risk is, however, a restrictive assumption. Variations in extra- and intracellular microenvironments, resulting from differences between cell types within an affected tissue, from deviations in the subcellular characteristics of cells of the same type, from exposure to different levels of diffusible factors, or from some combination thereof are likely to cause the risk to vary from cell to cell.

In this paper we develop and apply a generalized one-hit model of ND that accommodates inter-neuron differences in death risk. We find that this approach yields better fits to ND data compared to homogeneous MSS risk models and leads to the first quantitative description of the heterogeneity of cell loss kinetics. Population models based on Gaussian or normal distributions of the death risk value among affected neurons are eliminated in all but one case; instead, we recover risk heterogeneities distributed with marked positive skew and leptokurtic central tendencies, which are assessed quantitatively. We conclude that all the ND cases for which we have kinetic data can be described by relatively few patterns in the death risk distributions, and may therefore, share common kinetic mechanisms at the level of individual cell dropout. Thus, our study provides the first measures of death kinetic heterogeneity in neuronal populations that are consistent with one-hit attrition in a wide variety of neurodegenerative disorders.

2. Model and methods

Our exploration of the MSS hypothesis makes several biological assumptions regarding the degenerating cell populations. First, the size of the affected population at the beginning of the degenerative process is the same as that of an unaffected population, and that all affected cells enter the MSS at the same time. Furthermore, we assume that all mutations are fully penetrant and expressive, and that chemical or physical injuries affect all cells equally. Finally, we assume that the risk of cell death experienced by a given neuron remains constant throughout the course of the degenerative process.

Let C be the number of groups of cells having the same one-hit death risk r_i and characteristic lifetime $\tau_i = 1/r_i$ where the integer index i labels the cell groups with $i = 1, \ldots, C$. The number $N(t)$ of cells remaining at time t is then given by the sum of one-hit exponential decay functions

$$N(t) = N_0 \sum_{i=1}^{C} \mathrm{e}^{-t/\tau_i} \rho(\tau_i) \tag{1}$$

where N_0 is the initial number of cells in the population, $N(t)$ is the number of neurons remaining at time t, and $\rho(\tau_i)$ represents the proportion of the cell population in which the characteristic lifetime is τ_i. $\rho(\tau_i)$ is, therefore, the frequency distribution of characteristic lifetimes within the degenerating population, with $\sum_i \rho(\tau_i) = 1$. For a large population in which the range of risk parameter values is effectively continuous, the sum (1) generalizes to

$$N(t) = N_0 \int_0^{\infty} \mathrm{e}^{-t/\tau} \rho(\tau)\, \mathrm{d}\tau \tag{2}$$

where $\rho(\tau_i)$ now represents the normalized continuous frequency distribution of the characteristic lifetimes across the population. Because many of the ND cases we examined are consistent with models in which the degenerative process starts after samples were first collected [5], we were also interested in a form of (2) that includes a delay parameter:

$$N(t) = \begin{cases} N_0 & t \leq \text{delay} \\ N_0 \displaystyle\int_0^{\infty} \mathrm{e}^{-(t-\text{delay})/\tau} \rho(\tau)\, \mathrm{d}\tau & t > \text{delay} \end{cases} \tag{3}$$

The death risk factor heterogeneity of each ND disorder population is fully characterized by $\rho(\tau_i)$. Since the $\rho(\tau_i)$ distribution has not previously been determined for any neuronal population undergoing cell death, we elected to obtain the first estimates reported here by fitting (2) and (3) to our ND data sets using a range of analytical models for $\rho(\tau_i)$ (see Table 1). The $\rho(\tau_i)$ models were chosen to incorporate the qualitative expectation that the distribution of death risk will

in general possess a population mode, but that the tails of the distribution may not be symmetric. The $\rho(\tau_i)$ were also chosen to explore one-sided as well as two-sided distributions of risk combined with a wide range of modal τ values. The normal (Gaussian) distribution was, therefore, selected as a candidate lifetime distribution to reflect the potential role of stochastic fluctuations of reactants localized to environments that are effectively at thermodynamic equilibrium. Likewise, both the Weibull and log-normal distributions were chosen due to their applicability in the analysis of the probabilities of failure in complex systems, such as biochemical pathways, where events are organized into sequential chains [26,43]. Finally, the exponential and half-normal distributions were chosen to represent highly skewed distributions, and were included for completeness.

The resulting models were programmed in Mathematica 4.2 (Wolfram Research, Inc., Champaign, IL), and least squared-fitting performed using the built-in non-linear regression analysis functions (Levenberg–Marquardt method [27]) that minimize the difference between each ND data set and Eqs. (2) and (3). The fitting algorithm was considered to have returned an important result if all parameter estimates were significantly different from zero at a p-level of 0.05. The resulting best-fit characteristic lifetime distributions were plotted, and their best-fit shape parameter values used to calculate the distribution mean, mode, standard deviation, coefficient of variation, skewness, and kurtosis. Of these, the coefficient of variation was used as a measure of risk heterogeneity that could be compared among different ND cases, and the skewness as a measure of distribution asymmetry.

To the best of our knowledge, the data suitable for quantitative studies of neuronal death kinetics comprise, at this time, 16 cases, including photoreceptor degeneration (10 inherited, 1 acquired) [4,12,15,22,23,32–34,36], amyotrophic lateral sclerosis (ALS) [8] and Parkinson's disease (PD) [14], a chemically-induced model of parkinsonism in the rat [35], excitotoxic death of cultured hippocampal neurons [11], and the loss of cerebellar granule cells secondary to the genetically determined loss of their target Purkinje cells in the brains of *Purkinje cell degeneration* (*Pcd*$^{-/-}$) mutant mice [39]. All were assessed with the heterogeneous one-hit model.

3. Results

As measured by the maximal coefficient of determination, R^2, the heterogeneous risk model outperformed the assumption of homogeneous or uniform one-hit death risk in 13 of the 16 cases (81% of cases; Table 2). In 14 of the 16 cases we obtained significant fits with at least one of the five $\rho(\tau_i)$ distributions considered (Table 2). Two of the three cases in which the homogeneous risk model gave superior performance, therefore, corresponded to ND data for which none of the five $\rho(\tau_i)$ gave a significant fit. The maximal R^2 ranged between 0.722 and 0.998 when considered across all ND cases and distribution models. On average, heterogeneous risk explained 4% more of the data variability than did uniform risk. The largest such difference was observed for the *Rcd* mutant data, in which the best-fit variable risk model could account for an additional 12% of the data spread.

A comparatively small difference in R^2 was observed between the heterogeneous and the homogeneous risk models when we analyzed the ND kinetics of cultured hippocampal neurons and the photoreceptors of *Pcd*$^{-/-}$ mutant mice. The data from patients in the clinical phase of PD was best-fit by the homogeneous risk model, which could account for 4% more of the data variability than the heterogeneous risk models. Thus, the cases in our sample for which the risk of neuronal death varies across the population significantly outnumber those for which the cell death risk is essentially uniform (13 versus 3 cases, respectively, i.e. 81% of cases accounted for by heterogeneous risk versus 19% of cases by uniform risk).

To determine whether one specific distribution function $\rho(\tau_i)$ always produced the best results when a significant fit was obtained by the heterogeneous risk model, we compared the R^2 values (Table 2) resulting from each significant fit. For the inherited photoreceptor degeneration (IPD) cases (10 data sets) the Weibull distribution provided the best-fit in seven cases, the log-normal distribution in one case, and the homogeneous or uniform risk model in two cases. In the physicochemical injury cases (two data sets) best performance was achieved with the log-normal distribution. For the brain degeneration cases (four data sets) the Weibull distribution pro-

Table 1
Distributions used in the fitting procedure, and equations used in calculation of the distribution statistics

Distribution $\rho(\tau)$	Equation[a]	Skewness[b]	Kurtosis[b]
Normal (Gaussian)	$\rho(\tau) = \frac{e^{-(\tau-\mu)^2/2\sigma^2}}{\sigma\sqrt{2\pi}}$	0	3
Log-normal	$\rho(\tau) = \frac{e^{-((\ln(\tau)-\mu)^2/2\sigma^2)}}{\sigma\tau\sqrt{2\pi}}$	$\gamma_1 = \frac{\tau_3}{(\sigma^2)^{3/2}}$	$\beta_2 = \frac{\tau_4}{(\sigma^2)^2}$
Half-normal	$\rho(\tau) = \frac{2\beta e^{-\beta^2\tau^2/\pi}}{\pi}$	1	3.87
Exponential	$\rho(\tau) = \beta e^{-\beta\tau}$	2	9
Weibull	$\rho(\tau) = e^{(\tau/\beta)^\alpha}\alpha\sigma^{-\alpha}\tau^{\alpha-1}$	$\gamma_1 = \frac{\tau_3}{(\sigma^2)^{3/2}}$	$\beta_2 = \frac{\tau_4}{(\sigma^2)^2}$

[a] μ, mean; σ, standard deviation; α, shape parameter; and β, scale parameter.

[b] τ_i, the ith moment of the distribution $\rho(\tau)$, is defined as $\tau_i = \int_{-\infty}^{\infty} \tau^i \rho(\tau)\, d\tau$.

Table 2
Coefficients of determination (R^2)[a] resulting from non-linear fits of ND cell loss data to heterogeneous or uniform one-hit risk models

ND model	Normal	Exponential	Half-normal	Log-normal	Weibull	Uniform risk
IPD						
Albino mice	0.84	0.739	0.533	0.85	**0.862**	0.814
Nr$^{-/-}$ mice[c]	0.89	0.871	0.838	n.s.[b]	**0.916**	0.852
Rds$^{-/-}$ mice	0.907	0.906	0.908	0.906	**0.908**	0.900
Rds$^{+/-}$ mice (delay)	0.929	0.912	0.901	0.929	**0.933**	0.886
Rom1$^{-/-}$ mice	0.838	0.674	0.682	0.854	**0.856**	0.815
Pd miniature schnauzer (delay)	0.961	0.947	0.935	0.98	**0.985**	0.943
Rcd Irish setter (delay)	0.84	0.711	0.681	**0.838**	n.s.	0.724
Pcd$^{-/-}$ photoreceptors (delay)	0.976	0.968	0.973	0.975	**0.976**	0.974
Rd$^{-/-}$ mice (delay)	n.s.	n.s.	n.s.	n.s.	n.s.	**0.814**
Rd$^{-/-}$;*Rds*$^{-/-}$ mice (delay)	n.s.	n.s.	n.s.	n.s.	n.s.	**0.909**
Physicochemical injury						
Retinal detachment[c]	0.891	0.902	0.895	**0.91**	0.905	0.878
Rat parkinsonism (delay)[c]	n.s.	0.973	0.956	**0.995**	0.995	0.886
Brain degeneration						
ALS (delay)	0.997	0.997	0.991	0.996	**0.998**	0.982
Cultured hippocampal cells	**0.985**	0.94	0.956	n.s.	n.s.	0.984
Pcd$^{-/-}$ granule cells (delay)	0.978	0.973	0.977	0.976	**0.977**	0.970
Parkinson's disease	n.s.	0.694	**0.722**	n.s.	n.s.	0.764

[a] All reported R^2 values were statistically significant ($p < 0.05$). The highest values are indicated in bold. Where indicated, a delay parameter was included in the model (see Section 2).
[b] n.s., not significant.
[c] Fits were performed on mean values. For further information regarding data sets, see [5,6] and references therein.

duced the best-fit in two cases, the normal distribution in one case. The remaining brain degeneration data set was best modeled by uniform risk.

Thus, no single distribution consistently yielded the best fits to all the available data. In 9 of the 14 ND cases (64%) in which there was a significant fit by at least one of the $\rho(\tau_i)$, the Weibull lifetime distribution produced the best-fit (Table 2). Seven of these nine cases (78%) were examples of inherited photoreceptor degeneration (IPD). The other two were ALS and granule cell loss in *Pcd*$^{-/-}$ mice. One of the IPD data sets, the *Rcd* mutant Irish setter dogs, was best-fit by the log-normal distribution of risks.

A close inspection of Table 2 shows that the data from photoreceptor and granule cell loss in *Pcd*$^{-/-}$ mice, and from photoreceptor loss in the *Rcd* mutant dogs, yielded marginally higher R^2 values when fit to models based on a normal (Gaussian) distribution of characteristic lifetimes. However, the normal distribution parameters obtained by the fit model in each of these instances made the unrealistic prediction that many cells in the population either die effectively instantaneously or have a characteristic lifetime $\tau < 0$. Consequently, the normal distribution was excluded as a candidate descriptor for the characteristic lifetime heterogeneity in these cases and optimal performance on the data assigned to the Weibull distribution (two cases: photoreceptor and granule cell loss in *Pcd*$^{-/-}$ mice) and the log-normal distribution (one case: *Rcd* mutant dogs).

A log-normal distribution of death risk values also produced the best fits to the ND data from physically or chemically invasive procedures, i.e. for photoreceptor detachment and for chemically-induced parkinsonism in the rat, respectively. Thus, in 12 of the 13 ND cases (i.e. 92% of the cases) consistent with a heterogeneous distribution of underlying one-hit death risk values, the best $\rho(\tau_i)$ identified by our modeling procedure was either the Weibull (nine cases) or the log-normal distribution (three cases). In fact, whenever they produced a significant fit at all, their R^2 values were never more than 0.005 (Weibull) or 0.012 (log-normal) lower than the corresponding value given by the best-fit distribution for that ND case.

A single case of CNS degeneration, the death of cultured hippocampal neurons due to exposure to excess amounts of neurotransmitter, fit best to a normal distribution of the one-hit death risk. In contrast to the three cases discussed above for which the normal distribution resulted in unrealistic values (zero and negative) of the characteristic lifetime, those of the hippocampal neurons gave a negligible proportion of neurons for which the predicted risk values fell in the non-physical range. The final ND case we examined, the death of neurons in the substantia nigra of patients with PD, was unique in that its best heterogeneous risk model was the half-normal distribution (Table 1); for this case, however, the homogeneous risk model returned data fits superior to the best of our heterogeneous risk models (Table 1).

The range of R^2 values observed for the *photoreceptor dysplasia* (*Pd*) data, an IPD affecting miniature schnauzers, was 0.05, indicating that the best and worst heterogeneous risk models differed in the amount of data variability that could be explained by 5%. Intriguingly, all five of the alternative $\rho(\tau_i)$ distributions resulting from fits of Eq. (3) to the schnauzer *Pd* data (i.e. the normal, exponential, half-normal, log-normal, and Weibull forms of $\rho(\tau_i)$; Table 2) were closely

similar in shape once optimized: the proportion of neurons with a particular characteristic lifetime τ rose steeply as τ increased to its modal value, and then declined more slowly throughout the remainder of the MSS risk range. That all five alternative distributions were able to fit the *Pd* data well, and were of similar shape once fit, suggested to us that the behavior of the best-fit risk distribution should be compared across the 13 ND cases in which the heterogeneous risk model outperformed the homogeneous risk model.

We, therefore, plotted the best-fit $\rho(\tau_i)$ distribution for each case (Figs. 1–3) and evaluated their moment properties as described above (Table 3). The results were striking. In all but one case (12/13 cases; 92%) the optimized behavior of the characteristic lifetime distribution visualized in the plots resembled that of the *Pd* schnauzers: a rapid rise to a peak at comparatively small risk values, followed by an asymmetric decline over a longer tail. All 12 of these distributions were either Weibull or log-normal (see above). Moment evaluation (Table 3) confirmed quantitatively the general trends in $\rho(\tau_i)$ behavior visualized in the figures, i.e. all 12 cases are characterized by marked positive skew and pronounced leptokurtosis.

Neuronal death in cultured hippocampal neurons followed a markedly different pattern of risk heterogeneity. In contrast to the strongly skewed $\rho(\tau_i)$ identified in all the other cases of heterogeneous risk there was a pronounced symmetric peak (Fig. 3b) fit best by a normal distribution.

To examine whether the IPD, the physicochemical injury, and the brain degeneration classes of ND data could be distinguished on the basis of the degree of risk heterogeneity associated with their neuronal attrition, we calculated the coefficient of variation for each best-fit distribution (Table 3) and used the Wilcoxon rank sum test to compare them across the three classes of data sets. The degree of risk heterogeneity was significantly higher ($p = 0.048$) in the IPDs than in brain ND, indicating the photoreceptor microenvironment has a more varied effect on the kinetics of ND than does the cellular environment of the brain.

4. Discussion

Our analysis has demonstrated that cell loss kinetics in the majority of ND cases (13 of 16, or 81%)for which loss

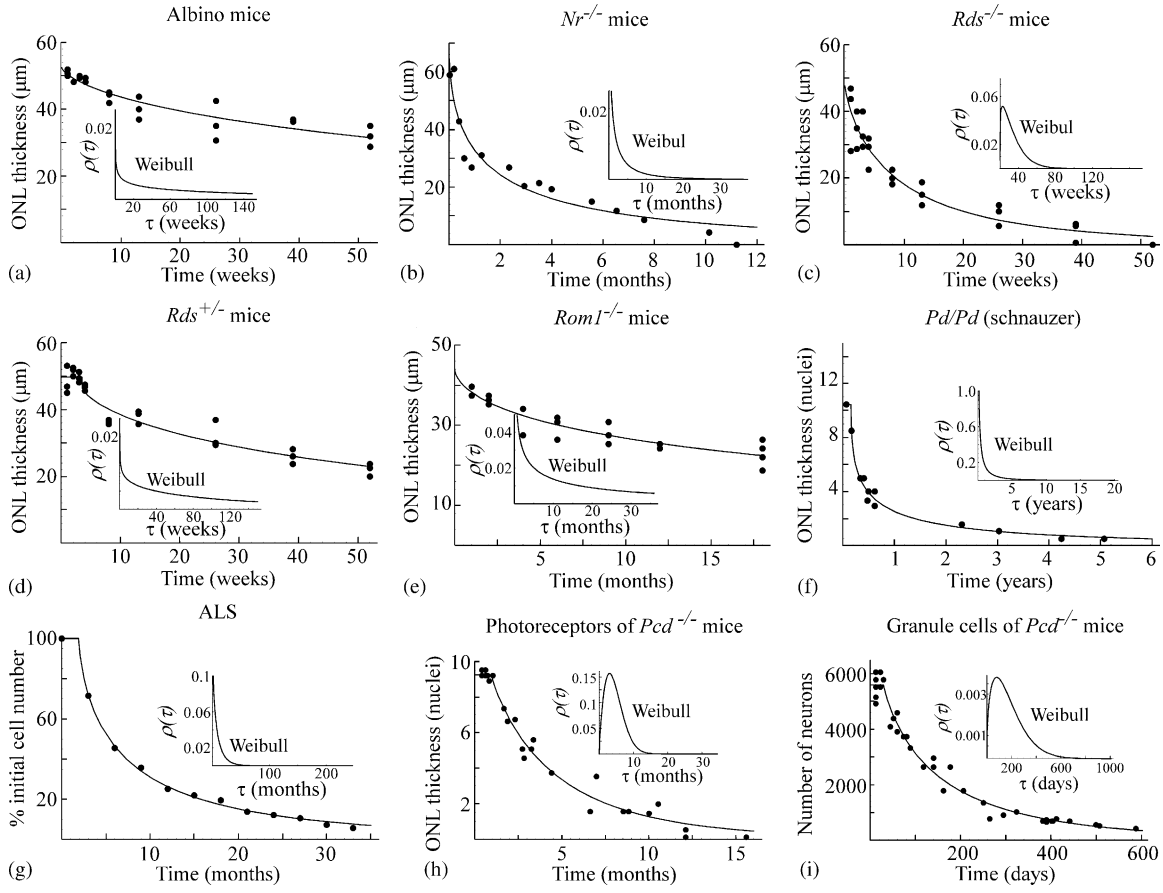

Fig. 1. The kinetics of neuronal loss in the majority of cases of ND are best described by heterogeneous risk models. Six examples of inherited photoreceptor degeneration (IPD) in mice (a–e and h), one case of IPD in miniature schnauzer dogs (f), the decline in evoked motor potentials an indirect measure of the number of motor units in patients with amyotrophic lateral sclerosis (ALS) (g), and the degeneration of granule cells in $Pcd^{-/-}$ mice (f) were best-fit using a Weibull distribution of cellular lifetimes. Each panel depicts the observed data and the degeneration curves resulting from the best-fit lifetime distribution (inset). ONL, retinal outer nuclear layer.

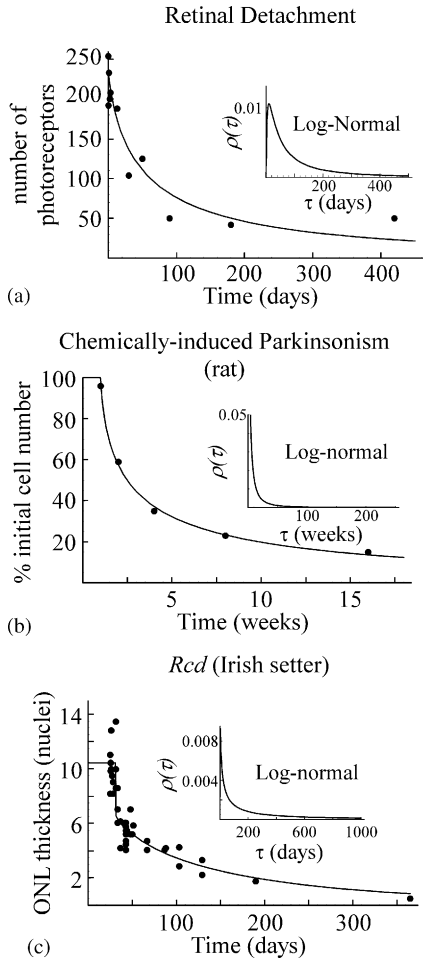

Fig. 2. The examples of ND resulting from physiochemical injury (a and b), and the degeneration of photoreceptors in Rcd dogs (c) were best-fit with a log-normal distribution of cellular lifetimes. ONL, retinal outer nuclear layer.

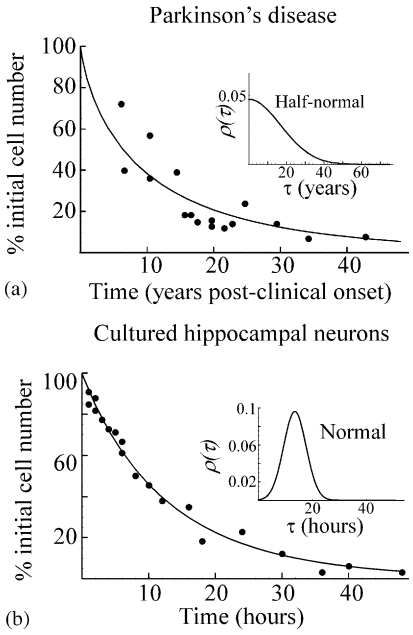

Fig. 3. The loss of neurons due to Parkinson's disease was best described using a Half-normal lifetime distribution (a), and the loss of cultured hippocampal neurons undergoing excitotoxic degeneration, the only example of in vitro ND, was best-fit using a normal distribution (b).

kinetics are known can be explained better by a heterogeneous risk mechanism than by models which assume that all neurons die under the same one-hit risk [5,6]. For them, the characteristic lifetime distribution $\rho(\tau_i)$, quantifies the variability in the risk parameter of the one-hit death process, and therefore, provides quantitative measures of the heterogeneity in cell dropout kinetics within the population. We find that incorporating this heterogeneity in a generalized version of our original one-hit model [5] increases the accuracy with which the available data can be explained.

The two most successful $\rho(\tau_i)$ functions in our analysis, the Weibull and log-normal distributions, best described 13 (93%) of the 14 ND cases for which the heterogeneous risk model resulted in significant fits to the data. Both are, therefore, candidate descriptors of the underlying cellular heterogeneity. Moreover, the success of the two distributions is consistent with biochemical knowledge regarding the protein networks controlling cell death. A Weibull distribution of one-hit risk implies that for a neuron to commit to cell death, all that is required is that one of many possible biochemical reactions maintaining the mutant steady state fail [43]. Similarly, the ability of a log-normal distribution in the one-hit risks to explain ND data is compatible with the involvement of a large number of relatively independent, stochastic biochemical events that must execute in succession [26] to trigger neuronal death. The strong showing of these distributions in neuronal death risk analysis, in which ND is triggered from biochemical events organized into complex nets of reaction paths [16], is therefore, consistent with the hypothesis that MSS accelerates cell attrition (compared the normal state of cell viability) through chemical changes that shift the modal frequency of cell failure to shorter times [5,6].

The Weibull and log-normal distributions have previously been reported to describe the diversity of a number of morphological measures of cell structure. For example, the distribution of both the soma size of rabbit retinal ganglion cells and the dendritic length of granular neurons from the human dentate gyrus can be accounted for by a Weibull function [30]. Likewise, the nuclear mass, volume and size have been shown to fit to log-normal distributions [1]. Whether there is any connection between the distribution types found for these measures of cell structure and the success of the Weibull and log-normal distributions in explaining our ND data is at present unclear. However, our present analysis makes important quantitative predictions regarding the parameters characterizing the neuronal lifetime distribution (Table 3), thereby allowing for direct comparisons to these morphological features, and indeed any cellular characteristic for which such measurements can be made. Such comparisons will permit the identification of those attributes of degenerating neuronal tissues that regulate the kinetics of cell loss.

Table 3
Parameter estimates and distribution statistics for best-fit lifetime distributions

ND model	Best-fit lifetime distribution $\rho(\tau)$	Parameter estimates (p-value)	Distribution statistics				
			Mean (months)	Standard deviation (months)	CoV	Skewness	Kurtosis
IPD							
Albino mice	Weibull ($F(2,25) = 3567.38$)	$\alpha = 0.75$ ($p < 0.001$), $\beta = 310.60$ ($p < 0.001$)	92.22	124.15	134.62	3.10	18.73
Nr$^{-/-}$ mice	Weibull ($F(2,13) = 234.53$)	$\alpha = 0.61$ ($p < 0.001$), $\beta = 2.88$ ($p < 0.001$)	4.26	7.35	172.72	4.47	38.35
Rds$^{-/-}$ mice	Weibull ($F(2,25) = 410.73$)	$\alpha = 1.16$ ($p < 0.001$), $\beta = 14.81$ ($p < 0.001$)	3.51	3.03	86.14	1.59	6.59
Rds$^{+/-}$ mice (delay)	Weibull ($F(2,25) = 2810.05$)	$\alpha = 0.84$ ($p < 0.001$), $\beta = 148.94$ ($p < 0.001$)	40.98	49.35	120.43	2.63	14.00
Rom1$^{-/-}$ mice	Weibull ($F(2,20) = 1942.49$)	$\alpha = 0.61$ ($p < 0.001$), $\beta = 69.00$ ($p < 0.002$)	101.63	174.98	172.20	4.45	38.00
Pd miniature schnauzer (delay)	Weibull ($F(2,10) = 926.80$)	$\alpha = 1.16$ ($p < 0.001$), $\beta = 14.81$ ($p < 0.001$)	14.88	34.68	234.18	7.11	102.55
Rcd Irish setter (delay)	Log-normal ($F(2,45) = 774.68$)	$\mu = 5.76$ ($p < 0.001$), $\sigma = 2.40$ ($p < 0.02$)	188.55	3349.8	1776.59	5660.71	1.01×10^{10}
Pcd$^{-/-}$ photoreceptors (delay)	Weibull ($F(2,22) = 1500.6$)	$\alpha = 1.72$ ($p < 0.001$), $\beta = 5.01$ ($p < 0.001$)	4.47	2.68	59.96	0.85	3.73
Physicochemical injury							
Retinal detachment (cat)	Log-normal ($F(2,9) = 247.57$)	$\mu = 4.27$ ($p < 0.001$), $\sigma = 1.40$ ($p < 0.002$)	6.41	15.90	248.27	22.75	3520.15
Rat parkinsonism (delay)	Log-normal ($F(2,3) = 1123.84$)	$\mu = 0.92$ ($p < 0.003$), $\sigma = 1.81$ ($p < 0.004$)	3.20	16.01	501.14	140.89	502684
Brain degeneration							
ALS (delay)	Weibull ($F(2,10) = 5638.98$)	$\alpha = 0.88$ ($p < 0.001$), $\beta = 9.30$ ($p < 0.001$)	9.91	11.28	113.87	2.42	12.18
Pcd$^{-/-}$ granule cells (delay)	Weibull ($F(2,33) = 2138.14$)	$\alpha = 1.41$ ($p < 0.001$), $\beta = 193.22$ ($p < 0.001$)	5.87	4.23	72.16	1.91	4.82
Cultured hippocampal cells	Normal ($F(2,17) = 1996$)	$\mu = 13.59$ ($p < 0.001$), $\sigma = 4.17$ ($p < 0.002$)	13.62 h	2.37 h	17.42	0	3
Parkinson's disease	Half-normal ($F(2,15) = 142.67$)	$\beta = 0.074$ ($p < 0.001$)	161.28	121.8	75.55	1.00	3.87

All reported p-values are significant ($p < 0.001$).

It is also encouraging to note that the initial characterization of $\rho(\tau_i)$ reported here is relevant to numerical methods aimed at identifying the best $\rho(\tau_i)$ for specific ND datasets. In principle, a procedure of inverse Laplace transformation, applied to Eq. (2), will by definition map any ND dropout dataset D into the lifetime frequency distribution $\rho(\tau_i)$ most closely associated with it. In general, however, such integral transform inversions must be carried out computationally, and the inversion algorithms require careful application in the case of well-skewed, long-tailed distributions like many of our $\rho(\tau_i)$ [9]. The results reported here are, therefore, a first step toward the definitive mapping of the one-hit ND risk distributions that best characterize the time course of specific neuronal attritions.

Despite the need for further computational progress, our results provide an initial general picture of the death risk heterogeneity relevant to the vast majority of ND cases thus far reported. Consistently across our analysis, we find risk distributions that rise quickly to the modal risk value at a relatively narrow peak and then decline more slowly, over a long tail. In view of these findings we anticipate that highly leptokurtic distributions with strong positive skew will be of wide applicability as the fundamental pattern by which death risk is distributed in neuronal populations. Further investigation will be needed to establish whether similar $\rho(\tau_i)$ regulate cell death in non-neuronal tissues, in normal developmental as well as in pathogenic processes.

A single ND data set—cultured hippocampal neurons exposed to excitotoxic levels of a glutamate—bucked this trend and defined a class of cell attrition in which the death risk distribution is highly symmetric. Until additional instances of this class are observed speculation about the origin of the associated $\rho(\tau_i)$ would be premature. However, it is interesting to note that the stochastic fluctuations of reactants are expected to be normally distributed in micro-environments that are effectively at thermodynamic equilibrium [29]. A direction for future work will be to establish whether the lifetime distribution of all degenerating neurons varies depending on whether the preparation is in vivo or in vitro, and if so, to determine how various sources of extracellular heterogeneity affect ND kinetics.

The data sets for the three cases best-fit by the uniform constant risk model (Table 2) are all unusual in some respect. The degeneration rate observed for the *Rd*$^{-/-}$ and *Rd*$^{-/-}$; *Rds*$^{-/-}$ mouse mutants was extremely rapid in the early stages of degeneration but substantially slower after most of the cells had died. It is possible that the distributions used in our study were unable to generate such a rapid decline in cell number followed by an extended tail region. Likewise, patients from which the PD data was derived were all within the clinical phase of the disease; the data may represent only part of the entire degenerative process [6], and our results for them should, therefore, be treated as preliminary. Additional analyses using more comprehensive data sets and alternative $\rho(\tau_i)$ distribution functions may subsequently be able to determine whether heterogeneous or homogeneous

Table 4
Summary of homogeneous and heterogeneous risk distribution statistics

ND model	Best-fit distribution	τ (Mean ± S.D.) (months)	Homogeneous risk lifetime (see ref. [5]) (months)
IPD			
Albino mice	Weibull	92.22 ± 124.15	27.26
Nr$^{-/-}$ mice	Weibull	4.26 ± 7.35	3.60
Rds$^{-/-}$ mice	Weibull	3.51 ± 3.03	3.43
Rds$^{+/-}$ mice (delay)	Weibull	40.98 ± 49.35	14.71
Rom1$^{-/-}$ mice	Weibull	101.63 ± 174.98	31.65
Pd (delay)	Weibull	14.88 ± 34.68 years	5.4
Rcd (delay)	Log-normal	188.55 ± 3349.8 days	2.00
Pcd$^{-/-}$ photoreceptors (delay)	Weibull	5.50 ± 2.68	5.11
Physicochemical injury			
Photoreceptor detachment	Log-normal	6.41 ± 15.90	4.43
Rat parkinsonism (delay)	Log-normal	3.20 ± 16.01	1.21
Brain degeneration			
ALS (delay)	Weibull	9.91 ± 11.28	9.83
Pcd$^{-/-}$ granule cells (delay)	Weibull	5.87 ± 4.23	5.56
Cultured hippocampal cells	Normal	13.62 ± 2.37 h	12.94 h
Parkinson's disease	Half-normal	161.28 ± 121.8	139.92

risk models are most accurate in describing ND in these examples.

For all the remaining ND cases, in which death risk was distributed heterogeneously, the lumped estimate of risk obtained from best fits of the uniform risk model to the data does not establish the pattern of risk variation (for which the risk distribution $\rho(\tau_i)$ must be evaluated rather than a single characteristic lifetime τ applicable to all cells in the population). Moreover, the uniform death risk τ so obtained agrees only approximately with first moment measures of $\rho(\tau_i)$, such as the mean death risk value, especially for the more heterogeneous ND cases such as IPD (Table 4). The heterogeneous risk model should, therefore, be regarded as a significant improvement in understanding the general kinetics of neuronal cell death.

Potential sources of cellular heterogeneities important to ND kinetics remain speculative and might include the variable abundances and localizations of the different cell types present within a tissue. For example, the cells of the hippocampus, a structure containing more than 10 types of interneurons, pyramidal, granule and glial cells [42] may display differences in their death kinetics that are related to variations in the biochemical constituents of the different cell types. However, our observation that the cell death risk distribution, and therefore, the risk-related environmental variation, is greater in IPD that in brain NDs (even though relatively few cell types are localized to the layer of the retina affected in IPDs) suggests that cell type diversity alone cannot account for the variation we have observed in the risk of neuronal death.

Individual neurons of the same cell type might also show variations in subcellular characteristics that affect ND kinetics. The architecture of dendritic arbors, axons, and the synaptic connections made by individuals neurons are highly variable and lead to differences in the expression levels and localization of neurotransmitters and receptors between otherwise equivalent neurons [7]. Additionally, the non-uniform distribution of diffusible factors in the extracellular environment, combined with their ability to affect the rate and spatial pattern of cell loss [2,10,19,21,28,37] provides a source of heterogeneity that could regulate cell death kinetics. Consequently, it is likely that each cell in a degenerating population is exposed to and responds to a somewhat unique microenvironment that shapes a distribution of cellular death risks.

Acknowledgment

This work has been supported by a grant to C.J.L. from the National Science and Engineering Research Council of Canada (NSERC). G.C. is a Canadian Institutes of Health Research (CIHR) Postdoctoral Fellow.

References

[1] G.F. Bahr, U.V. Mikel, The distribution of nuclear mass, volume and dimensions, Anal. Quant. Cytol. 7 (1985) 119–125.
[2] J. Burns, G. Clarke, C.J. Lumsden, Photoreceptor death: spatiotemporal patterns arising from one-hit death kinetics and a diffusible cell death factor, Bull. Math. Biol. 64 (2002) 1117–1145.
[3] D.B. Carr, A. Goate, J.C. Morris, Current concepts in the pathogenesis of Alzheimer's disease, Am. J. Med. 103 (1997) 3S–10S.
[4] G. Clarke, A.F.X. Goldberg, D. Vidgen, L. Collins, L. Schwarz, L. Ploder, L.L. Molday, J. Rossant, R.S. Molday, D.G. Birch, R.R. McInnes, Rom-1 is required for rod photoreceptor viability and the regulation of disk morphogenesis, Nat. Genet. 25 (2000) 67–73.
[5] G.A. Clarke, R.A. Collins, B.R. Leavitt, D.F. Andrews, M.R. Hayden, C.J. Lumsden, R.R. McInnes, A one-hit model of cell death in inherited neuronal degenerations, Nature 406 (2000) 195–199.
[6] G.A. Clarke, C.J. Lumsden, R.R. McInnes, Inherited neurodegenerative diseases: the one-hit model of neurodegeneration, Hum. Mol. Genet. 10 (2001) 2269–2275.
[7] A.M. Craig, H. Boudin, Molecular heterogeneity of central synapses: afferent and target regulation, Nat. Neurosci. 4 (2001) 569–578.

[8] M. Dantes, A. McComas, The extent and time course of motoneuron involvement in amyotrophic lateral sclerosis, Muscle Nerve 14 (1991) 416–421.
[9] B. Davies, B. Martin, Numerical inversion of the Laplace transform: a survey and comparison of methods, J. Comp. Phys. 33 (1979) 1–32.
[10] D. Dawbarn, S.J. Allen, Neurotrophins and neurodegeneration, Neuropathol. Appl. Neurol. 29 (2003) 211–230.
[11] J.M. Dubinsky, B.S. Kristal, M. Elizondo-Fournier, On the probabilistic nature of excitotoxic neuronal death in hippocampal neurons, Neuropharmacology 34 (1995) 701–711.
[12] P.A. Erickson, S.K. Fisher, D.H. Anderson, W.H. Stern, G.A. Borgula, Retinal detachment in the cat: the outer nuclear and outer plexiform layers, Invest. Ophthalmol. Vis. Sci. 24 (1983) 927–942.
[13] R.L. Ernst, J.W. Hay, The US economic and social costs of Alzheimer's disease revisited, Am. J. Public Health 84 (1994) 1261–1264.
[14] J.M. Fearnley, A.J. Lees, Ageing and Parkinson's disease: substantia nigra regional selectivity, Brain 114 (1991) 2283–2301.
[15] R.K. Hawkins, H.G. Jansen, S. Sanyal, Development and degeneration of the retina in rds mutant mice: photoreceptor abnormalities in the heterozygotes, Exp. Eye Res. 41 (1985) 701–720.
[16] M.O. Hengartner, The biochemistry of apoptosis, Nature 407 (2000) 770–776.
[17] M.A. Hickey, M.-F. Chesselet, Apoptosis in Huntington's disease, Prog. Neuro-Psychopharmacol. Biol. Psychol. 27 (2003) 255–265.
[18] D.E. Hobson, Clinical manifestations of Parkinson's disease and parkinsonism, Can. J. Neurol. Sci. 30 (2003) S2–S9.
[19] P. Huang, A. Gaitan, Y. Hao, R.M. Peters, F. Wong, Cellular interactions implicated in the mechanism of widespread photoreceptor degeneration in transgenic mice expressing a mutant rhodopsin gene, Proc. Natl. Acad. Sci. U.S.A. 90 (1993) 8484–8488.
[20] M.E. Illing, M.S. Rajan, N.F. Bence, R.R. Kopito, A rhodopsin mutant linked to autosomal dominant retinitis pigmentosa is prone to aggregate and interacts with the ubiquitin proteasome system, J. Biol. Chem. 277 (2002) 34150–34160.
[21] W. Kedzierski, D. Bok, G.H. Travis, Non-cell autonomous photoreceptor degeneration in rds mutant mice mosaic for expression of a rescue transgene, J. Neurosci. 18 (1998) 4076–4082.
[22] M.M. LaVail, J.C. Blanks, R.J. Mullen, Retinal degeneration in the pcd cerebellar mouse. I. Light microscopic and autoradiographic analysis, J. Comp. Neurol. 212 (1982) 217–230.
[23] M.M. LaVail, M.P. White, G.M. Gorrin, D. Yasumura, K.V. Porrello, R.J. Mullen, Retinal degeneration in the nervous mouse. I. Light microscopic cytopathology and changes in the interphotoreceptor matrix, J. Comp. Neurol. 333 (1993) 168–181.
[24] N. Lev, E. Melamed, D. Offen, Apoptosis and Parkinson's disease, Prog. Neuropsychopharmacol. Biol. Psychiatry 27 (2003) 245–250.
[25] F.-Q. Liang, B.F. Godley, Oxidative stress-induced mitochondrial DNA damage in human retinal pigment epithelial cells: a possible mechanism for RPE aging and age-related macular degeneration, Exp. Eye Res. 76 (2003) 397–403.
[26] E. Limpert, W.A. Stahel, M. Abbt, Log-normal distributions across the sciences: keys and clues, Bioscience 51 (2001) 341.
[27] D.W. Marquardt, An algorithm for least-squares estimation of nonlinear parameters, J. Soc. Ind. Appl. Math. 11 (1963) 431–441.
[28] S. Mohand-Said, A. Deudon-Combe, D. Hicks, M. Simonutti, V. Forster, A.-C. Fintz, T. Leveillard, H. Dreyfus, J.-A. Sahel, Normal retina releases a diffusible factor stimulating cone survival in the retinal degeneration mouse, Proc. Natl. Acad. Sci. U.S.A. 95 (1998) 8351–8356.
[29] G. Nicolis, I. Prigogine, Self-organization in Nonequilibrium Systems: From Dissipative Structures to Order Through Fluctuations, John Wiley & Sons, New York, 1977.
[30] C.W. Oyster, E.S. Takahashi, D.C. Hurst, Analysis of neuronal soma size distributions, J. Neurosci. Methods 6 (1982) 311–326.
[31] L.R. Pacione, M.J. Szego, S. Ikeda, P.M. Nishina, R.R. McInnes, Progress toward understanding the genetic and biochemical mechanisms of inherited photoreceptor degenerations, Ann. Rev. Neurosci. 26 (2003) 657–700.
[32] C.J. Parshall, M. Wyman, S. Nitroy, G. Acland, G. Aguirre, Photoreceptor dysplasia: an inherited progressive retinal atrophy of miniature schnauzer dogs, Prog. Vet. Comp. Ophthalmol. 1 (1991) 187–203.
[33] S. Sanyal, R.K. Hawkins, Genetic interaction in the retinal degeneration of mice, Exp. Eye Res. 33 (1981) 213–222.
[34] S. Sanyal, R.K. Hawkins, Absence of photoreceptor outer segments in the retina of rds mutant mice, Neurosci. Lett. 21 (1981) 23–26.
[35] H. Sauer, W.H. Oertel, Progressive degeneration of nigrostriatal dopamine neurons following intrastriatal terminal lesions with 6-hydroxydopamine: a combined retrograde tracing and immunocytochemical study in the rat, Neuroscience 59 (1994) 401–415.
[36] S.Y. Schmidt, G. Aguirre, Reductions in taurine secondary to photoreceptor loss in Irish setters with rod-cone dysplasia, Invest. Ophthalmol. Vis. Sci. 26 (1985) 679–683.
[37] G.S. Seigal, L. Liu, Inducible apoptosis-promoting activity in retinal cell-conditioned medium, Mol. Vision 3 (1997) 14.
[38] C. Soto, Unfolding the role of protein misfolding in neurodegenerative diseases, Nat. Rev. Neurosci. 4 (2003) 50–60.
[39] L.C. Triarhou, Rate of neuronal fallout in a transsynaptic cerebellar model, Brain Res. Bull. 47 (1998) 219–222.
[40] C.M. Troy, G.S. Salvesen, Caspases on the brain, J. Neurosci. Res. 69 (2002) 145–150.
[41] M. Vila, S. Prezborski, Targeting programmed cell death in neurodegenerative diseases, Nat. Rev. Neurosci. 4 (2003) 1–11.
[42] E. Vreugdenhil, E.R. de Kloet, M. Schaaf, N.A. Datson, Genetic dissection of corticosterone receptor function in the rat hippocampus, Eur. Neuropsychopharmacol. 11 (2001) 423–430.
[43] W. Weibull, A statistical distribution function of wide applicability, J. Appl. Mech. 18 (1951) 293–297.

Available online at www.sciencedirect.com
SCIENCE DIRECT®
Journal of Theoretical Biology 233 (2005) 515–525
Journal of Theoretical Biology
www.elsevier.com/locate/yjtbi

Scale-free neurodegeneration: cellular heterogeneity and the stretched exponential kinetics of cell death

Geoff Clarke, Charles J. Lumsden*

Department of Medicine, University of Toronto, Medical Sciences Building, 1 King's College Circle, Room 7313, Toronto, Canada M5S 1A8

Received 4 April 2004; received in revised form 25 October 2004; accepted 28 October 2004
Available online 19 December 2004

Abstract

Neurodegenerative disorders are an insidious group of diseases characterized by severe physical and cognitive effects that often have devastating consequences for the lives of affected individuals and their families. One feature common to a significant proportion of these diseases is that affected neurons commit to undergoing an active form of degeneration known as programmed cell death, or apoptosis. Although intense effort over the past several years has resulted is a remarkable increase in our understanding of the molecular events involved in neurodegeneration, our knowledge regarding the cellular and tissue properties that determine the temporal patterns of neuronal attrition is limited. We recently demonstrated that neurodegenerative kinetics in various diseases fit well to exponential decay functions, and proposed a universal one-hit switch mechanism in which mutant and injured neurons exist in a viable state characterized by an increased but constant risk of initiating apoptosis (Nature, 406, p. 195). Here we show that a heavy-tailed stretched exponential function is better able to account for neurodegenerative kinetic data. Moreover, normalization of all available data according to their corresponding best-fit stretched exponential parameters suggest that the generalized model is consistent with a universal mechanism of neuronal cell death that is greatly improved over the constant risk model. In contrast to the original model in which all cells exhibit an identical risk of initiating apoptosis, the stretched exponential model is consistent with each neuron experiencing a constant risk that is different from that experienced by other cells in the degenerating population, perhaps due to spatial differences in the cellular microenvironment. Intriguingly, the predicted distribution of risk across the cell population can be fit by a power-law function, further suggesting that scale-free properties of degenerating neuronal tissues might act as potent regulators of the kinetics of cell death in neural tissue.

Keywords: Neurodegeneration; Heterogeneity; Stretched exponential; Scale free; Mutant steady state

1. Introduction

Neurodegenerative diseases are a varied group of disorders that normally strike later in life, frequently with debilitating physical and cognitive effects on the lives of affected individuals. For example, Alzheimer's disease, the most common form of disease-causing neurodegeneration (ND), affects approximately 1% of individuals between the ages of 65 and 69 years, and close to 50% of people over the age of 95. This devastating disorder results primarily in cognitive difficulties for affected individuals—symptoms include a progressive decline in memory, decision making and language skills, and increasing disorientation to surroundings (Nussbaum and Ellis, 2003). In contrast, diseases such as amyotrophic lateral sclerosis (ALS, or Lou Gerhrig's disease) result primarily in physical difficulties—ALS patients present with muscle weakness and alterations in their reflexes, which manifest as paralysis, speech and swallowing difficulties, and ultimately respiratory failure leading to death within 2–5 years of diagnosis (Guégan and Przedborski, 2003). In addition to the personal costs borne by affected

*Corresponding author. Tel.: +1 416 978 7178; fax: +1 416 978 3701.
E-mail addresses: geoff.clarke@utoronto.ca (G. Clarke), charles.lumsden@utoronto.ca (C.J. Lumsden).

0022-5193/$ - see front matter © 2004 Elsevier Ltd. All rights reserved.
doi:10.1016/j.jtbi.2004.10.028

individuals and their families, the direct and indirect economic toll resulting from neurodegenerative diseases is substantial. According to one estimate, costs associated with treating Alzheimer's disease are on the order of $70 billion dollars per year (1991 currency) in the United States alone (Carr et al., 1997; Ernst and Hay, 1994), a value that will increase as the population ages.

Detailed knowledge regarding the genetic and environmental causes of ND has increased dramatically in recent years. Whereas few causes of inherited ND were known a decade ago, mutations in a growing number of genes are now known to be involved in various forms of neurodegenerative disease, including Parkinson's (at least 10 genes; Dawson and Dawson, 2003) and Alzheimer's disease (4 genes; Kennedy et al., 2003), ALS (7 major genes; Majoor–Krakeuer et al., 2003), and the heterogeneous group of inherited photoreceptor degenerations (IPDs; over 150 genes, http://www.sph.uth.tmc.edu/Retnet/, and Pacione et al., 2003). The mechanisms by which these primary genetic insults lead to the death of individual neurons are, however, still poorly understood. For example, mutations in genes encoding proteins responsible for maintaining cell structure, for regulating the expression of other genes, and for signal transduction have all been associated with various forms of ND. This diversity in putative ND effectors has led to proposals regarding the molecular mechanism of neuronal cell death initiation that range from a gradual accumulation of cellular damage caused by the production of oxygen radicals (Ischiropoulos and Beckman, 2003; Klein and Ackerman, 2003), to protein misfolding and the associated accumulation of intracellular aggregates to toxic levels (Soto, 2003).

An important property of ND that has received far less attention than the molecular characterization of its effectors is the kinetics by which neurons are lost from the affected cell population. We have previously demonstrated that the kinetics of neuronal loss in many forms of both inherited and acquired ND can be described by a one-hit process in which the risk of death averaged across the cell population is a constant over time (Clarke et al., 2000, 2001). To account for this observation, we hypothesized the existence of an alternative homeostatic state of cell function, the *mutant steady state* (MSS), in which the injured and mutant neurons are viable but at an increased risk of initiating cell death compared to normal neurons. This increase in risk may arise, for example, due to a shift in the abundance of critical pro-death molecules—normal stochastic fluctuations in the abundance of these molecules may drive individual neurons past a threshold beyond which cell death ensues.

For several of the ND cases examined in our previous work (Clarke et al., 2000, 2001), the cell death curves corresponding to the constant risk model declined toward zero at a rate greater than that exhibited by the experimental data, suggesting that models able to generate a heavy-tailed cell drop-out curve may better reflect the underlying degenerative mechanisms. Support for this possibility is provided by the original analysis, which demonstrated that several ND examples fit better to an exponentially decreasing risk model of cell death. One such heavy-tailed function is the stretched exponential, or Kohlrausch–Williams–Watts (KWW) (Alvarez et al., 1991; Lee et al., 2001) function

$$\phi(t) = \exp(-t/\tau_{KWW})^{\beta}$$

frequently used in the analysis of electronic and molecular relaxation (Bendler and Shlesinger, 1985, 1987; Klafter and Shlesinger, 1986; Shlesinger and Montroll, 1984). Also known as the Weibull function (Weibull, 1951), the stretched exponential has also been regularly used for lifetime analysis of components in complex systems. Additionally, the stretched exponential function has been used to describe fluorescence lifetimes in heterogeneous biological samples.

In this paper we demonstrate that the stretched exponential is also well suited to the description of neuronal cell death in complex tissues. Intriguingly, we find that the heavy-tailed decay of the stretched exponential neural death is compatible with a generalized one-hit cell death model, in which death risk varies from cell to cell. These finding hold for all cases of neurodegeneration in which death kinetics data are available. Furthermore, we demonstrate that the distribution of cellular lifetimes corresponding to the best-fit stretched exponential model for all ND examples can be described by a power law, suggesting that scale-free properties of the affected tissues are critical regulators of the kinetics of ND.

2. Model and methods

The number of neurons remaining at time t in a tissue degenerating according to a stretched exponential process is given by

$$N(t) = N_0 \exp(-t/\tau_{KWW})^{\beta}, \tag{1}$$

where N_0 is the initial number of neurons in the population, τ_{KWW} measures the characteristic time-scale of the decay process, and β is a shape parameter such that $N(t)$ yields a power-law function as $\beta \to 0^+$, $\beta = 1$ equates to the original homogeneous constant risk model, and $\beta > 1$ results in sigmoidal decay. Because many of the ND cases we examined are consistent with models in which the degenerative process starts after samples were first collected, we were also interested in a

form of Eq. (1) that includes a delay parameter

$$N(t) = \begin{cases} N_0, & t \leqslant delay, \\ N_0 \exp(-(t - delay)/\tau_{KWW})^{\beta}, & t > delay. \end{cases} \quad (2)$$

Neurodegenerative kinetics consistent with the stretched exponential function $N(t)$ can also be described by

$$N(t) = N_0 \int_0^{\infty} \exp(-t/\tau_i)\rho(\tau)\,d\tau, \quad (3)$$

where each neuron is characterized by a one-hit risk of cell death r_i and a characteristic lifetime $\tau_i = 1/r_i$, and the variation in cell death risk across each ND population is completely described by $\rho(\tau)$, the normalized continuous frequency distribution of characteristic lifetimes (Liebovitch and Tóth, 1991; Lindsey and Patterson, 1980), where

$$\rho(\tau) = -\frac{\tau_{KWW}}{\pi\tau^2} \sum_{k=0}^{\infty} \frac{(-1)^k}{k!} \sin\,\pi\beta k \Gamma(\beta k + 1) \left(\frac{\tau}{\tau_{KWW}}\right)^{\beta k+1} \quad (4)$$

$$= \frac{1}{\pi} \int_0^{\infty} e^{-\tau x - \lambda x^{\beta} \cos(\beta\pi)} \sin[\lambda x^{\beta} \sin(\beta\pi)]\,dx \quad (5)$$

and $\lambda = 1/\tau_{KWW}^{\beta}$ and $0 < \beta \leqslant 1$.

To evaluate the ability of the stretched exponential function to describe ND kinetic data, we first fit Eqs. (1) and (2) to our ND data sets using the built-in nonlinear regression analysis functions (Levenberg–Marquardt method; Marquardt, 1963) of Mathematica 5.0 (Wolfram Research Inc., Champaign, IL), and compared the results to those produced by the original homogeneous constant risk (HCR) and exponentially decreasing risk (HEDR) models (Clarke et al., 2000, 2001). In view of the well documented problems in accurately computing $\rho(\tau)$ from Eqs. (4) and (5) (Lindsey and Patterson, 1980), we also calculated the inverse Laplace transform of (3) using the best-fit stretched exponential parameters and the Mathematica GWR package utilizing the Gaver–Stahfest method (Valko and Vajda, 2002) (http://library.wolfram.com/infocenter/MathSource/4738/), and compared the results to those from Eqs. (4) and (5). For each method, a range of τ values spanning 3 orders of magnitude was evaluated, up to a maximum equal to either the approximate lifespan of the affected organism (mice, 3 years; rat, 3 years; schnauzer, 15 years, Irish setter, 14 years, cat, 15 years; or human, 85 years) or the duration of the degenerative period as predicted by the stretched exponential best-fit equations. For some ND examples (see Table 2), solutions over this range of values were unstable, and results were therefore calculated across a smaller parameter range.

We analysed all ND cases known to us for which the data allowed the examination of neuronal loss over a sufficiently large range of the degenerative period. In most cases, this range spanned times early enough in the degenerative process so that little or no significant cell death could be observed, to times at which either no further cell loss can be measured or the affected population has been depleted of all cells. Sixteen cases were studied (for primary ND data sources, see Clarke et al., 2000, 2001), including photoreceptor degeneration (10 inherited, 1 acquired), amyotrophic lateral sclerosis (ALS) and Parkinson's disease (PD), a chemically induced model of parkinsonism in the rat, excitotoxic death of cultured hippocampal neurons, and the loss of cerebellar granule cells secondary to the genetically determined loss of their target purkinje cells in the brains of Purkinje cell degeneration ($Pcd^{-/-}$) mutant mice. All were assessed with the methods described above.

3. Results

All three models were able to give significant fits to at least some of the ND sets (Table 1). Although the HEDR model provided the highest coefficients of determination in 25% of all ND cases studied, its inability to fit a further 25% of ND cases indicated that an exponentially decreasing risk model does not reflect a general unifying mechanism of ND. In contrast, both the stretched exponential and HCR functions produced significant regression results for all cases. However, the stretched exponential function consistently produced higher R^2 values than those of the HCR model: those values resulting from fits to the stretched exponential model ranged between 0.764 and 0.998 (Table 1, Fig. 1), whereas the values corresponding to the HCR model were between 0.724 and 0.984. On average, the stretched exponential model was able to account for an additional 4% of the ND data variability than was the HCR model; the largest difference being observed for the *Rcd/Rcd* dog mutant, for which the stretched exponential model could explain 11% more of the data spread.

Given that both the stretched exponential and the HCR models fit every ND case examined, it is possible that the models reflect an underlying universal mechanisms of neuronal cell death. To evaluate the possible universality of the original HCR model, we first tested our original conjecture that the HCR model indicates that ND can be viewed as a discrete birth–death Markov process, much like radioactive decay (Clarke et al., 2000). Given an exponentially decreasing random variable $X(t)$, the expected value and variance are given, respectively, by

$$\langle X(t) \rangle = X_0 \exp\left[\frac{-(t - t_0)}{\tau}\right], \quad (6)$$

$$var\,\{X(t)\} = X_0 \exp\left[\frac{-(t - t_0)}{\tau}\right] \left(1 - \exp\left[\frac{-(t - t_0)}{\tau}\right]\right), \quad (7)$$

Table 1
Coefficients of determination (R^2)[a] and best-fit parameters for the homogeneous constant risk (HCR), Homogeneous exponentially decreasing risk (HEDR) and stretched exponential models of neuronal cell attrition

ND model	Homogeneous constant risk (HCR)[b]	HCR characteristic lifetime	Homogeneous exponentially decreasing risk (HEDR)[b]	HEDR parameters ($\tau_0 \equiv$initial lifetime, $\alpha \equiv$rate const of lifetime decay)	Stretched exponential	Stretched exponential parameters
Photoreceptor degeneration						
Albino mice	0.814	$\tau = 109.00$ weeks	0.877[c]	$\tau_0 = 37.04$ weeks, $\alpha = 0.068$	0.870	$\tau_{KWW} = 201.34$ weeks, $\beta = 0.41$
Nr$^{-/-}$ mice	0.852	$\tau = 3.59$ months	0.879	$\tau_0 = 1.43$ months, $\alpha = 0.366$	0.916	$\tau_{KWW} = 1.87$ months, $\beta = 0.49$
Photoreceptors of *Pcd*$^{-/-}$ mice	0.974[c]	$\tau = 4.37$ months	0.962	$\tau_0 = 3.07$ months, $\alpha = 0.083$	0.976[c]	$\tau_{KWW} = 3.89$ months, $\beta = 0.82$
Pd/*Pd* (miniature schnauzer)	0.943	$\tau = 0.45$ years	0.978[c]	$\tau_0 = 0.336$ years, $\alpha = 1.13$	0.985[c]	$\tau_{KWW} = 0.36$ years, $\beta = 0.41$
Rcd/*Rcd* (Irish setter)	0.724[c]	$\tau = 48.85$ days	0.823[c]	$\tau_0 = 17.24$ days, $\alpha = 0.043$	0.833[c]	$\tau_{KWW} = 47.23$ days, $\beta = 0.30$
Rd$^{-/-}$; *Rds*$^{-/-}$ mice	0.909[c]	$\tau\tau = 8.15$ days	n.s.	n/a	0.984[c]	$\tau_{KWW} = 3.83$ days, $\beta = 0.35$
Rd$^{-/-}$ mice	0.814[c]	$\tau = 4.81$ days	n.s.	n/a	0.928	$\tau_{KWW} = 14.42$ days, $\beta = 9.17$
Rds$^{-/-}$ mice	0.900	$\tau = 13.72$ weeks	0.903	$\tau_0 = 8.93$ weeks, $\alpha = 0.034$	0.908	$\tau_{KWW} = 10.77$ weeks, $\beta = 0.71$
Rds$^{+/-}$ mice	0.886	$\tau = 58.91$ weeks	0.909	$\tau_0 = 31.25$ weeks, $\alpha = 0.033$	0.933[c]	$\tau_{KWW} = 86.13$ weeks, $\beta = 0.50$
*Rom*1$^{-/-}$ mice	0.815	$\tau = 31.61$ months	0.857	$\tau_0 = 14.71$ months, $\alpha = 0.099$	0.855	$\tau_{KWW} = 37.89$ months, $\beta = 0.52$
Physicochemical damage						
Retinal detachment	0.878	$\tau = 67.88$ days	0.929	$\tau_0 = 43.48$ days, $\alpha = 0.014$	0.902	$\tau_{KWW} = 75.90$ days, $\beta = 0.59$
Chemically induced parkinsonism (rat)	0.886	$\tau = 4.83$ weeks	0.997[c]	$\tau_0 = 1.86$ weeks, $\alpha = 0.301$	0.995[c]	$\tau_{KWW} = 3.26$ weeks, $\beta = 0.48$
Peripheral nerve degeneration						
ALS	0.982	$\tau = 9.45$ months	0.996	$\tau_0 = 7.52$ months, $\alpha = 0.035$	0.998[c]	$\tau_{KWW} = 6.39$ months, $\beta = 0.61$
Brain degenerations						
Cultured hippocampal neurons	0.984	$\tau = 12.93$ h	n.s.	n/a	0.985	$\tau_{KWW} = 13.09$ h, $\beta = 0.95$
Granule cells of *Pcd*$^{-/-}$ mice	0.97	$\tau = 169.28$ days	0.969[c]	$\tau_0 = 131.58$ days, $\alpha = 0.0018$	0.978[c]	$\tau_{KWW}\tau = 143.88$ days, $\beta = 0.76$
Parkinson's disease	0.764	$\tau = 11.66$ years	n.s.	n/a	0.764	$\tau_{KWW} = 11.62$ years, $\beta = 0.98$

n.s., not significant; n/a, not applicable.
[a]All reported R^2 values are statistically significant ($P > 0.01$).
[b]For relevant equations, please see (Clarke et al., 2000).
[c]Fits were done to models which included a delay parameter.

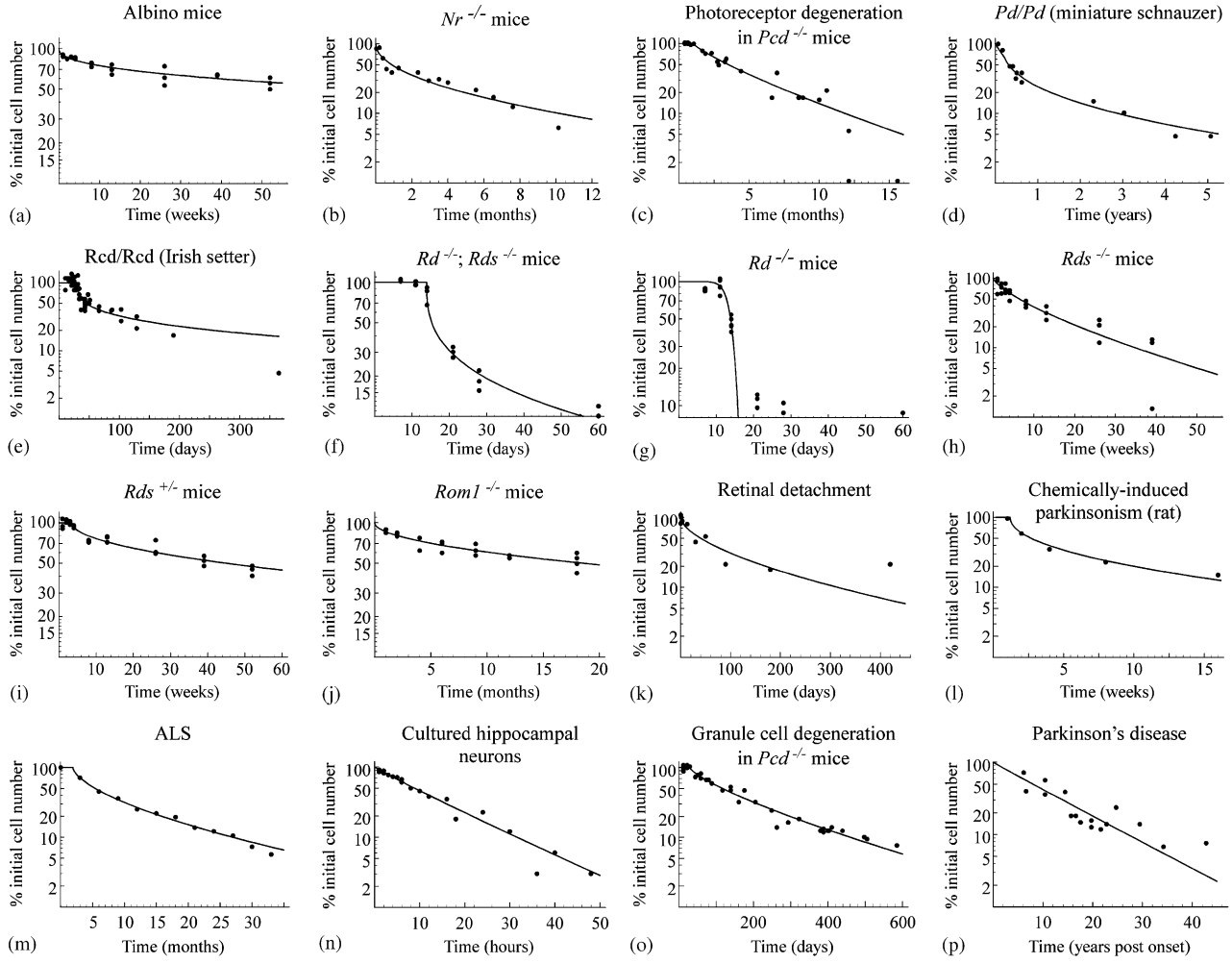

Fig. 1. The stretched exponential function provides significant fits to all cases of neurodegeneration for which appropriate data sets exist. Semi-log plots of the best-fit curves, along with data points, are shown for the 16 cases for which appropriate data were available. (a–j) Loss of cells, measured by either direct nuclear counting or by the thickness of the retinal outer nuclear layer, resulting from 10 cases of inherited photoreceptor degeneration (IPD). Loss of neurons due to physicochemical damage was measured by direct counts of both photoreceptors in cats with experimentally detached retinas (k) and of dopamine neurons in the nigrostriatim of a chemically induced rat model of Parkinson's disease (l). Peripheral nerve degeneration in patients with amyotrophic lateral sclerosis was measured by the decline in evoked motor potentials (m), while direct counts of cells were made in cultures of hippocampal neurons (n), of cerebellar granule cells in the $Pcd^{-/-}$ mutant mouse (o) , and of neurons in the caudal substantia nigra of patients with Parkinson's disease (p). For further details regarding these data sets, see Clarke et al. (2000, 2001) and references therein.

where X_0 is the initial value of the variable. Upon rearrangement, we obtain.

$$\frac{var\{X(t)\}}{\langle X(t)\rangle} = 1 - \langle X(t)\rangle \frac{1}{X_0.} \tag{8}$$

Thus, plots of $var\{X(t)\}/\langle X(t)\rangle$ vs. $1/\langle X(t)\rangle$ should be linear with a slope of $1/X_0$ and intercept of 1. Such plots were generated for the 7 ND cases for which multiple measurements were available at each timepoint, and linear regression performed on the resulting curves. In no case could the results be fit to a straight line (data not shown), indicating that ND cannot be viewed as a Markov process.

To further explore the nature of the stretched exponential and HCR models as universal descriptors of ND, we plotted the ND data sets normalized according to the best-fit parameter estimates from each model. If these functions describe general mechanisms of ND, then an appropriate normalization will eliminate a substantial degree of variability across all data sets. Whereas normalization according to the HCR best-fit parameters still produced widely varying degeneration curves (Fig. 2a), those resulting from normalization with the best-fit stretched exponential parameters are remarkably similar (Fig. 2b), indicating that the stretched exponential model provides an improved theoretical basis from which mechanisms of ND should be considered.

The ND examples we have analysed can be grouped into 4 clinically defined categories: inherited photore-

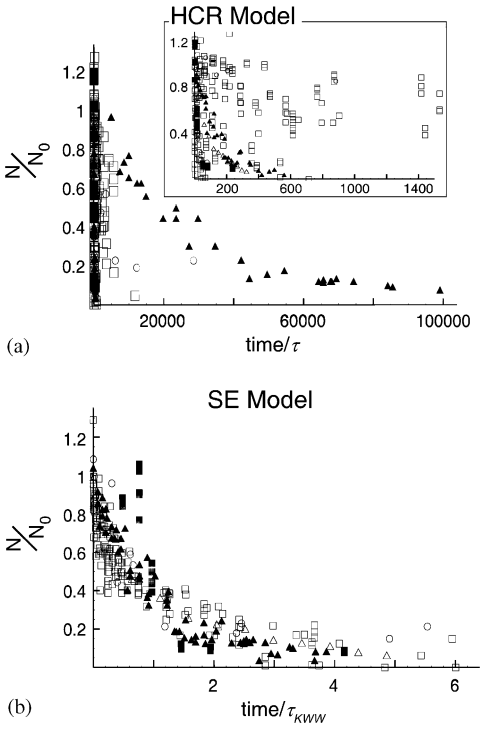

Fig. 2. Plots of data normalized to model parameters suggest that a stretched exponential mechanism has universal applicability in neurodegenerative disease. Data normalized to the HCR model parameters results in plots with a significant amount of scatter over a wide range of values. In contrast, plots of data normalized to the stretched exponential parameter estimates follow essentially a single curve (b). The example that exhibits the most variability in this plot is that of the $Rd^{-/-}$ mice, which also exhibited a b parameter value significantly greater than those of the other ND cases examined. Open squares, IPD cases; closed squares, photoreceptor degeneration in $Rd^{-/-}$ mutant mice; closed triangles, peripheral nerve degeneration (ALS); open circles, physicochemical damage.

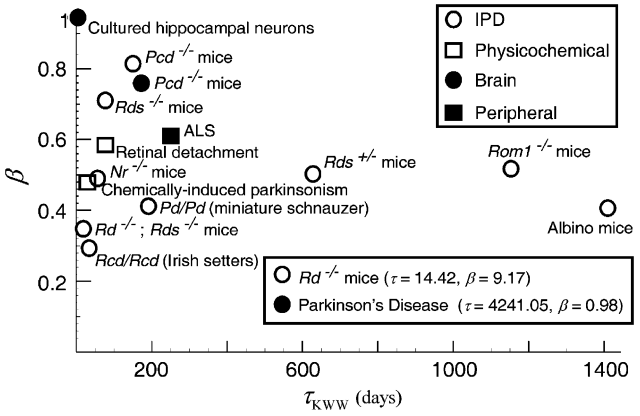

Fig. 3. A scatterplot of stretched exponential best-fit parameter values suggests that clinically distinct forms of ND exhibit different cell loss kinetics. All cases exhibited widely varying τ_{KWW} parameter values, whereas the IPD data is consistent with β values that were significantly lower than those of the brain degeneration examples.

ceptor degenerations (IPD), peripheral nerve degenerations, brain degenerations, and cases resulting from physicochemical damage. To determine if the stretched exponential best-fit parameter values mirror these clinical classifications, we generated a scatterplot of the stretched exponential parameters for all ND cases (Fig. 3). The ND examples from the IPD and brain degeneration categories were distributed across a wide range of characteristic lifetime τ_{KWW} values, while the corresponding values from the peripheral nerve degeneration and the two examples resulting from physicochemical disruption exhibited relatively short characteristic lifetimes. In contrast to this relatively uniform distribution of τ_{KWW} values, estimates of β appeared grouped according to type of ND in question: whereas $\beta > 0.75$ for all examples of brain degeneration, the vast majority ($\frac{10}{13}$, or 77%) of the remaining ND examples exhibited $\beta < 0.6$. These patterns in the parameter value scatterplot were supported by Mann–Whitney U and Wilcoxan W tests: a significant difference ($P = 0.018$) was observed only between the β values of the IPDs and brain degeneration examples.

The heavy tail of the stretched exponential function can also be generated by an infinite sum of exponential functions (see Eq. (3)) with a distribution of characteristic times given by $\rho(\tau)$. To explore how the individual characteristic lifetimes τ_i are distributed across the degenerating neuronal populations, we characterized $\rho(\tau)$ by calculating a numerical solution to the inverse Laplace transform of Eq. (3) using a Gaver–Stahfest algorithm (Valko and Vajda, 2002) and the stretched exponential parameter estimates corresponding to each ND example. For this analysis, data from the $Rd^{-/-}$ mouse mutant was excluded since the best-fit estimate of $b > 0$. For the majority of ND cases (12/15—all but photoreceptor degeneration in the $Nr^{-/-}$, $Pcd^{-/-}$, and Pd/Pd mutants), $\rho(\tau)$ decayed rapidly during the early period of the degeneration, and the decay rate continually slowed over the course of the degeneration. Logarithmic plots of τ vs. $\rho(\tau)$ appeared linear (Fig. 4) for all but one of the 12 cases, suggesting the presence of a power-law relationship. The case for which the logarithmic plot was not linear—cell loss due to Parkinson's disease (Fig. 4o)—is characterized by a linear regime at higher τ values ($\tau \gtrsim 3$ months) preceded by a short period of increasing slope in the logarithmic plot.

For the three remaining ND examples photoreceptor degeneration in the $Nr^{-/-}$, $Pcd^{-/-}$, and Pd/Pd mutant animals the calculated $\rho(\tau)$ rose sharply, reached a peak close to $\tau = 0$, and subsequently decayed according to a power law. For example, the $\rho(\tau)$ distribution of the Pd/Pd schnauzer mutants increased for a great enough period that a substantial proportion (approximately 37%) of the affected cells would undergo cell death before the degeneration enters the power-law phase.

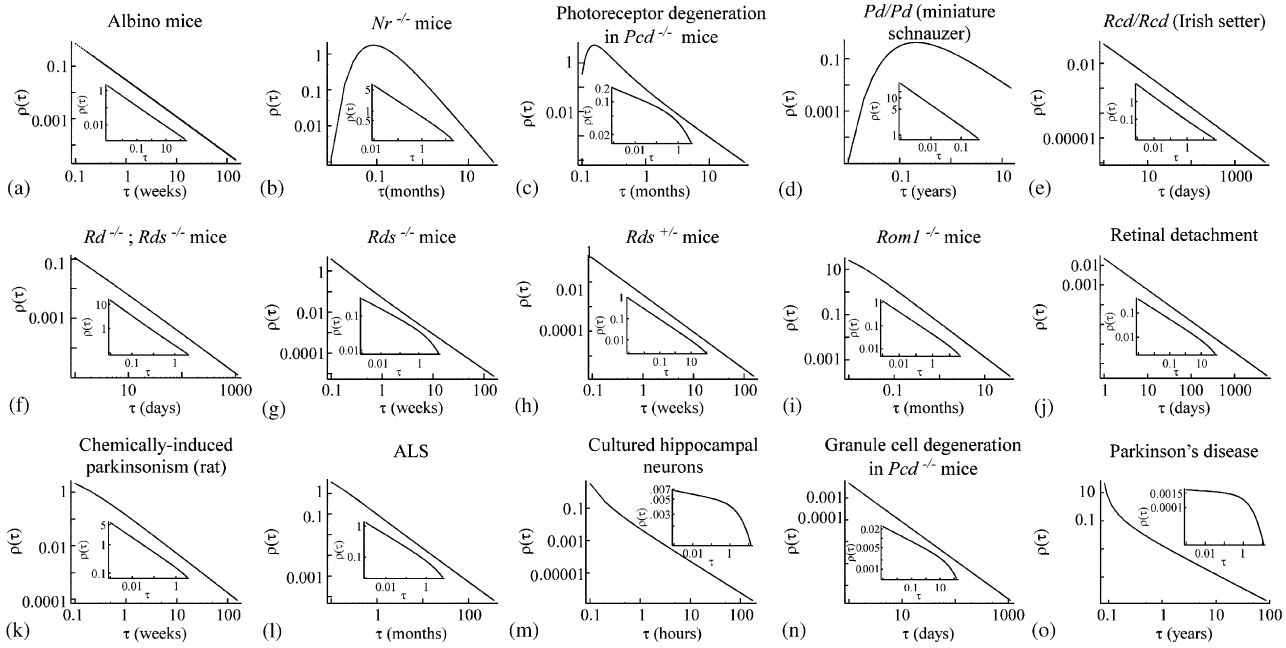

Fig. 4. Inverse Laplace transforms of the best-fit stretched exponential equations suggest that the distribution of cellular lifetimes in neurodegenerative diseases can be described by a power-law relationship. Two complementary methods were used to determine $\rho(\tau)$. Results from a numerical solution (Gaver–Stahfest algorithm) to the ILT for each ND case is shown in the main figure of each panel, whereas the corresponding results from the series approximation to the ILT solution are exhibited in panel insets. (a–i) IPD examples, excluding that from the $Rd^{-/-}$ mice. (j, k) physicochemical injuries. (l) ALS, affecting peripheral neurons. (m–o) brain degeneration examples.

However, the proportion of the degenerative time period for which $\rho(\tau)$ increases is not always so great: the peak value of $\rho(\tau)$ occurs at 2.1 and 4.8 days in the $Nr^{-/-}$ and $Pcd^{-/-}$ mouse mutants respectively whereas the degeneration of all photoreceptor cells in these animals requires on the order of 1 year to complete (Fig. 1).

Numerous numerical algorithms can be used to calculate ILTs (Davies and Martin, 1979; Valko and Vajda, 2002), and caution is required when using algorithms that have not been tested with a particular function of interest. Since we are unaware of numerical ILT techniques that have been verified for use with the stretched exponential function, we confirmed the results described above by using known analytical approximations to the stretched exponential ILT solution (Lindsey and Patterson, 1980). Over the same range of τ values explored for the numerical solutions, the results of the series approximation (see Eq. (4)) were stable for only four of the 15 ND cases analysed. For the remaining 11 cases, $\rho(\tau) \to \pm\infty$ as τ increased. Since it has been previously reported that difficulties with the precision of the series solution may be encountered when $\tau > \tau_{KWW}$ (Lindsey and Patterson, 1980), we recalculated $\rho(\tau)$ across this smaller domain and plotted the results. Results from 10 of the 15 ND cases examined, including 7 of the 9 IPD cases and all examples involving physicochemical and peripheral nerve damage, supported the possibility of power-law lifetime distributions in that the series approximation was linear, or very nearly linear on logarithmic plots (Fig. 4, insets). The remaining examples—photoreceptor loss in $Pcd^{-/-}$ and $Rds^{-/-}$ mice, Parkinson's disease, cultured hippocampal neurons, and granule cell loss in $Pcd^{-/-}$ mice—exhibited lifetime distributions that declined linearly over the early period of degeneration ($0.001 \leqslant \tau \lesssim 0.1\tau_{KWW}$) but that become increasingly steep as τ increased.

Estimates of $\rho(\tau)$ from 5 of the ND examples—the $Nr^{-/-}$, $Pcd^{-/-}$ and Pd/Pd IPD examples, and cell loss in cultured hippocampal neurons and due to Parkinson's disease (Fig. 4b–d, m, o, respectively)—were inconsistent with those produced by the numerical Gaver–Stahfest algorithm. For these cases, the shape of the lifetime distributions differed significantly over a similar range of τ values. An extreme example of this difference is observed for the Pd/Pd mutant schnauzer example (Fig. 4d): while the results corresponding to the series approximation of the stretched exponential ILT predict a power-law relationship over the range of $0.001 \leqslant \tau \leqslant \tau_{KWW} = 0.36$ years, results from the numerical method indicate that $\rho(\tau)$ increases between $0.01 \leqslant \tau \leqslant 0.22$ years.

To clarify the inconsistencies between these results, we also calculated an integral approximation to the stretched exponential ILT (see Eq. (5)) (Lindsey and Patterson, 1980) across the full range of τ values for all ND examples. In all cases, results of the integral approximation were virtually identical to those of the

Table 2
Power-law exponents[a] corresponding to three methods for solving the stretched exponential inverse Laplace transform

ND model	$\tau_{MIN} \leqslant \tau \leqslant \tau_{MAX}$	Gaver–Stahfest (numerical)	Series approximation ($0.001 \leqslant \tau \leqslant \tau_{KWW}$)	Integral approximation
Photoreceptor degeneration				
Albino mice	$0.1 \leqslant \tau \leqslant 156$ weeks	−1.40	−0.581	−1.40
$Nr^{-/-}$ mice	$0.01 \leqslant \tau \leqslant 36$ months	−1.38	−0.560	−1.38
Photoreceptors of $Pcd^{-/-}$ mice	$0.01 \leqslant \tau \leqslant 36$ months	−1.72 ($\tau_{MIN} = 0.03$ months)	−0.470	−1.93[b] ($\tau_{MIN} = 0.1$ months)
Pd/Pd (miniature schnauzer)	$0.01 \leqslant \tau \leqslant 15$ years	−0.912	−0.580	−0.912
Rcd/Rcd (Irish setter)	$1 \leqslant \tau \leqslant 5000$ days	−1.30	−0.621	−1.30
$Rd^{-/-}$; $Rds^{-/-}$ mice	$1 \leqslant \tau \leqslant 1095$ days	−1.33	−0.600	−1.33
$Rds^{-/-}$ mice	$0.1 \leqslant \tau \leqslant 156$ weeks	−1.73	−0.507	−1.73
$Rds^{+/-}$ mice	$0.1 \leqslant \tau \leqslant 156$ weeks	−1.50	−0.562	−1.50
$Rom1^{-/-}$ mice	$0.01 \leqslant \tau \leqslant 36$ months	−1.52	−0.559	−1.52
Physicochemical damage				
Retinal detachment	$1 \leqslant \tau \leqslant 5545$ days	−1.59	−0.547	−1.59
Chemically induced parkinsonism (rat)	$0.1 \leqslant \tau \leqslant 156$ weeks	−1.46	−0.567	−1.46
Peripheral nerve degeneration				
ALS	$0.1 \leqslant \tau \leqslant 360$ months	−1.62	−0.543	−1.62
Brain degenerations				
Cultured hippocampal neurons	$0.1 \leqslant \tau \leqslant 175$ h	−1.97	−0.393	−1.97
Granule cells of $Pcd^{-/-}$ mice	$1 \leqslant \tau \leqslant 1095$ days	−1.76	−0.494	−1.76
Parkinson's disease	$0.01 \leqslant \tau \leqslant 85$ years	−2.03 ($\tau_{MIN} = 0.085$ years)	−0.368	−2.03 ($\tau_{MIN} = 0.085$ years)

[a]All values are statistically significant ($P > 0.01$).
[b]Calculations performed over 2 orders of magnitude.

numerical solution (data not shown). To further explore the reproducibility of the ILT results, we calculated the power-law exponents resulting from each of the 3 methods by applying least-squares linear regression techniques to the corresponding estimates of $\rho(\tau)$. All methods resulted in significant linear fits, with a range in R^2 values of 0.825–0.999 for the series approximation, and 0.771–0.999 for the integral and numerical solutions. Overall, the power exponent values ranged between −0.368 and −0.621 according to the series approximation, and between −0.912 and −2.03 for both the Gaver–Stahfest numerical and the integral approximation approaches (Table 2). Importantly, the power exponents calculated according to the latter two methods were identical in all but one ND case, IPD in $Pcd^{-/-}$ mice. However, when results for this example were recalculated over identical domains ($0.1 \leqslant \tau \leqslant 36$ months) using the numerical and integral methods, the resulting power exponents were identical (data not shown), indicating that these methods yield uniform results across all ND cases.

4. Discussion

The stretched exponential function is able to produce curves varying between power-law ($\tau \approx 0$), exponential ($\tau = 1$), and sigmoidal decay ($\tau > 1$), and thus provides a flexible tool with which the kinetics of ND can be studied. Since it was first introduced almost 150 years ago, the relevance of stretched exponential decay has been demonstrated in remarkably diverse fields of study. For example, it has most often been analysed within the context of relaxation in electronic and molecular systems (Bendler and Shlesinger, 1985, 1987; Klafter and Shlesinger, 1986; Shlesinger and Montroll, 1984), but has also been used in the analysis of the kinetics of random network growth (Krapivsky et al., 2000), the distribution of extinction events, energy emissions from astrophysical sources, earthquake magnitude and geologic fault displacements, and currency value fluctuations (Laherrère and Sornette, 1998). Significantly for this study, the function has also been widely utilized in engineering analyses where measuring the reliability of complex systems and their components is critical in predicting system failures.

The ability of the stretched exponential function to accurately fit all known ND cases for which quantitative cell death kinetic data are available is compatible with the hypothesis that a universal underlying mechanism is responsible for the observed ND kinetics. This possibility is further supported by our demonstration that normalized ND data sets—encompassing the degeneration of at least 6 neuronal cell types in 5 regions of the

nervous system that result from both genetic and acquired insults in various organisms—exhibit a significant and surprising degree of overlap (Fig. 2). In contrast, the highly scattered nature of data normalized according to the HCR model parameters, along with our demonstration that the data are inconsistent with the idea that ND can be viewed as a birth–death Markov process, indicates that the universal explanatory abilities of the HCR model are limited.

A single ND case, photoreceptor loss in $Rd^{-/-}$ mice fit to Eq. (1) best with a parameter value of $\beta = 9.17$, exceeding the range in which the stretched exponential function is normally applied (Table 1). A possible explanation for this unique result is that the distribution of data for the $Rd^{-/-}$ mice, combined with the relatively rapid progression of cell death, lend themselves to fits with high β values, when in fact additional data may result in parameter estimates more in line with the other ND cases we examined. However, given that the rate of cell loss exhibited by the $Rd^{-/-}$; $Rds^{-/-}$ mice is comparable to that of the $Rd^{-/-}$ mice, we find this unlikely. An alternative interpretation based on studies of excitation transfer in condensed media suggests that β may be related to the fractal dimensionality of the system (Klafter and Shlesinger, 1986; Phillips, 1996, 2000). If this interpretation is applicable to ND systems, it implies that the mechanism resulting in stretched exponential decay for the $Rd^{-/-}$ case is of much higher dimensionality than the other cases in our analysis.

An important point to emphasize is that the superior explanatory ability of the stretched exponential model in no way invalidates the one-hit hypothesis—that a single intracellular event is responsible for the commitment to a degenerative process. Although additional explanations may fit with the observed kinetics (see below), our results make the important conceptual advance in the one-hit hypothesis that a model in which tissue heterogeneities generate different, yet constant risk values for each individual cell in the degenerating population (recall Eq. (3)) is better able to explain the kinetics of cell loss in examples of neurodegenerative disorders.

In their analysis of fluorescent lifetimes in biological samples, Lee et al. (2001) suggested that β reflects a measure of tissue heterogeneity. If so, then our observation that two clinically distinct classes of ND, IPDs and brain degenerations, exhibited a significant difference in their stretched exponential parameters suggest that the biochemical milieu of a degenerating brain is less complex (i.e. β close to 1) than the environment in which degenerating photoreceptors are located, at least with respect to the factors influencing cell death. This result is somewhat surprising given the differences in the composition of the respective tissues. If cell diversity, measured in terms of the number of major cell types represented in the degenerating population, is an important factor in determining environmental heterogeneity, a tissue containing few cell types would exhibit a higher value of β than one with a greater number of cell types. However, our results indicate that degeneration of cultured hippocampal cells, presumably consisting of a mix of the various interneurons, pyramidal, granule and glial cells known to exist within the hippocampus (Vreugdenhil et al., 2001), is consistent with a rather homogeneous environment (Table 1), while the stretched exponential parameters of IPD cases, involving only two types of photoreceptor cells, exhibits a higher degree of variability in the neuronal characteristic lifetimes. This result indicates that either an alternative explanation for the β measurements is required, or that the real source of death-related heterogeneity lies elsewhere.

One such source of heterogeneity may be the subcellular variations often exhibited by neurons of the same type. For example, the abundance and distribution of synaptic components are determined and maintained by communication between neurons across their synaptic connections (Craig and Boudin, 2001). The diversity in synaptic connectivity experienced by different cells therefore results in a corresponding variation in the abundance and distribution of neurotransmitters and receptors across cells in a degenerating neuronal population. Alternatively, a non-uniform distribution of diffusible substances, such as trophic or toxic factors within the extracellular environment may also affect the kinetics of cell loss in a complex tissue (Burns et al., 2002). Candidate factors might include oxygen-free radicals (Andersen, 2004), excess glutamate (Sattler and Tymianski, 2001), or calcium ions (Mattson, 2004), all compounds known to impact cell death. Analysis of cellular and tissue variations, and identification of factors able to modulate neuronal attrition rates may thus allow for the development of therapeutics able to mitigate the effects of these debilitating diseases.

The effort of identifying such regulatory factors will require detailed analysis of the distribution of tissue heterogeneities, and our elucidation of $\rho(\tau)$ is therefore an important first step in this process. The consistency between the results of the integral approximation and the Gaver–Stehfest numerical solution to the stretched exponential ILT suggests that they provide an accurate estimate of the cellular lifetime distribution. In those instances where $\rho(\tau)$ increased before decaying according to a power law, the peak in the distribution was observed at extremely low values of τ (data not shown)—usually before the time at which data were first collected and at a point when the best-fit stretched exponential function predicts that very few, if any of the affected of the neurons have undergone cell death. These results suggest that for all ND cases examined, the distribution of cellular lifetimes $\rho(\tau)$ can be best described by a power-law function, indicating that the

longer a neuron survives, the less likely it is to undergo cell death. However, this interpretation should be used with caution: the relevance of the power-law distribution in Nature is often called into question because the range of scaling behavior exhibited in experimental preparations is usually small (Laherrère and Sornette, 1998). Moreover, that the log-normal and power-law distributions can mimic each other over certain parameter ranges indicates that additional cell attrition data spanning a greater range of timescales will be required to confirm our results.

Numerous physical and biological processes have been demonstrated to exhibit stretched exponential decay kinetics, and any mechanism proposed to account for this behavior is a candidate that might also apply to the kinetics ND. Similar to the idea of tissue heterogeneity proposed by Lee et al. (2001) to account for the variation in fluorescent lifetimes, subcellular environmental variations on the scale of individual proteins may subtly alter the kinetics of individual proapoptotic reactions, resulting in variations in the time at which cells commit to cell death and producing the observed distribution in cellular lifetimes. Of equally interesting biological relevance are analyses in which the fluctuations between open and closed states of an ion channel are described by fractal kinetics rather than by a simple Markov process (Liebovitch et al., 1987; Liebovitch and Tóth, 1991). These analyses revealed that the probability of a such a channel remaining in a given state for time t decays according to a stretched exponential function. Intriguingly, a role for channels in the apoptotic cell death process has been suggested (Danial and Korsmeyer, 2004). A key event in the progression of apoptosis is the permeabilization of the mitochondrial membrane, allowing the release of cytochrome c into the cytoplasm where it can interact with other molecules to form the apoptosome. That the proapoptotic BCL-2 family members BAX and BAK are thought to form channels capable of eliciting this cytochrome c release suggests that scale free properties of such channels may be responsible for the generation of stretched exponential kinetics in neurodegenerative disease.

Mechanisms yielding stretched exponential decay in the physical sciences may also be relevant for the kinetics of neuronal cell loss. For example, the kinetics of relaxation in molecular and electronic glasses has been suggested to result from the trapping of excitations by random diffusible defects in the media (Bendler and Shlesinger, 1987). Mechanisms based on this idea might be relevant to neuronal death resulting from the diffusion of toxic substances through a degenerating tissue (Burns et al., 2002).

Alternatively, stretched exponential decay has been postulated to result from a hierarchical mechanism in which relaxation occurs according to a multiplicative process (Klafter and Shlesinger, 1986; Palmer et al., 1984): constraints at one level must be relieved before those at other levels can relax. Progression through a signal transduction cascade might represent such a sequence of events.

Acknowledgements

We gratefully acknowledge support provided in the form of a researched grant to CJL from the National Science and Engineering Research Council of Canada (NSERC). GC is a Canadian Institutes of Health Research (CIHR) Postdoctoral Fellow.

References

Alvarez, F., Alegría, A., Colmenero, J., 1991. Relationship between the time-domain Kohlrausch–Williams–Watts and frequency-domain Havriliak–Negami relaxation functions. Phys. Rev. B 44, 7306–7312.

Andersen, J.K., 2004. Oxidative stress in neurodegeneration: cause or consequence? Nat. Rev. Neurosci. 5, S18–S25.

Bendler, J.T., Shlesinger, M.F., 1985. Derivation of the Kohlrausch–Williams/Watts decay law from activation energy dispersion. Macromolecules 18, 591–591.

Bendler, J.T., Shlesinger, M.F., 1987. Defect-diffusion models of relaxation. J. Mol. Liq. 36, 37–46.

Burns, J., Clarke, G., Lumsden, C.J., 2002. Photoreceptor death: spatiotemporal patterns arising from one-hit death kinetics and a diffusible cell death factor. Bull. Math. Biol. 64, 1117–1145.

Carr, D.B., Goate, A., Morris, J.C., 1997. Current concepts in the pathogenesis of Alzheimer's disease. Am. J. Med. 103, 3S–10S.

Clarke, G., Collins, R.A., Leavitt, B.R., Andrews, D.F., Hayden, M.R., Lumsden, C.J., McInnes, R.R., 2000. A one-hit model of cell death in inherited neuronal degenerations. Nature 406, 195–199.

Clarke, G., Lumsden, C.J., McInnes, R.R., 2001. Inherited neurodegenerative diseases: the one-hit model of neurodegeneration. Hum. Mol. Genet. 10, 2269–2275.

Craig, A.M., Boudin, H., 2001. Molecular heterogeneity of central synapses: afferent and target regulation. Nat. Neurosci. 4, 569–578.

Danial, N.N., Korsmeyer, S.J., 2004. Cell death: critical control points. Cell 116, 205–219.

Davies, B., Martin, B., 1979. Numerical inversion of the Laplace transform: a survey and comparison of methods. J. Comp. Phys. 33, 1–32.

Dawson, T.M., Dawson, V.L., 2003. Molecular pathways of neurodegeneration in Parkinson's disease. Science 302, 819–822.

Ernst, R.L., Hay, J.W., 1994. The US economic and social costs of Alzheimer's disease revisited. Am. J. Publ. Health 84, 1261–1264.

Guégan, C., Przedborski, S., 2003. Programmed cell death in amyotrophic lateral sclerosis. J. Clin. Invest. 111, 153–161.

Ischiropoulos, H., Beckman, J.S., 2003. Oxidative stress and nitration in neurodegeneration: cause, effect, or association? J. Clin. Invest. 111, 163–169.

Kennedy, J.L., Farrar, L.A., Andreason, N.C., Mayeux, R., St George-Hyslop, P., 2003. The genetics on adult-onset neuropsychiatric disease: complexities and conundra? Science 302, 822–826.

Klafter, J., Shlesinger, M.F., 1986. On the order relationship among three theories of relaxation in disordered systems. Proc. Natl Acad. Sci. USA 83, 848–851.

Klein, J.A., Ackerman, S.L., 2003. Oxidative stress, cell cycle, and neurodegeneration. J. Clin. Invest. 111, 785–793.

Krapivsky, P.L., Redner, S., Leyvraz, F., 2000. Connectivity of growing random networks. Phys. Rev. Lett. 85, 4629–4632.

Laherrère, J., Sornette, D., 1998. Stretched exponential distributions in nature and economy: "fat tails" with characteristic scales. Eur. Phys. J. B 2, 525–539.

Lee, K.C.B., Siegel, J., Webb, S.E.D., Lévêque-Fort, S., Cole, M.J., Jones, R., Dowling, K., Lever, M.J., French, P.M.W., 2001. Application of the stretched exponential function to fluorescence lifetime imaging. Biophys. J. 81, 1265–1274.

Liebovitch, L.S., Fischbarg, J., Koniarek, J.P., 1987. Ion channel kinetics: a model based on fractal scaling rather than multistate Markov processes. Math. Biosci. 84, 37–68.

Liebovitch, L.S., Tóth, T.I., 1991. Distributions of activation energy barriers that produce stretched exponential probability distributions for the time spent in each state of the two state reaction $A \rightleftharpoons B$. Bull. Math. Biol. 53, 443–455.

Lindsey, C.P., Patterson, G.D., 1980. Detailed comparison of the Williams–Watts and Cole–Davidson functions. J. Chem. Phys. 73, 3348–3357.

Majoor-Krakeuer, D., Willems, P.J., Hofman, A., 2003. Genetic epidemiology of amyotrophic lateral sclerosis. Clin. Genet. 63, 83–101.

Marquardt, D.W., 1963. An algorithm for least-squares estimation of nonlinear parameters. J. Soc. Ind. Appl. Math. 11, 431–441.

Mattson, M.P., 2004. Pathways towards and away from Alzheimer's disease. Nature 430, 631–639.

Nussbaum, R.L., Ellis, C.E., 2003. Alzheimer's disease and Parkinson's disease. N. Engl. J. Med. 348, 1356–1364.

Pacione, L.R., Szego, M.J., Ikeda, S., Nishina, P.M., McInnes, R.R., 2003. Progress toward understanding the genetic and biochemical mechanisms of inherited photoreceptor degenerations. Ann. Rev. Neurosci. 26, 657–700.

Palmer, R.G., Stein, D.L., Abrahams, E., Anderson, P.W., 1984. Models of hierarchically constrained dynamics for glassy relaxation. Phys. Rev. Lett. 53, 958–961.

Phillips, J.C., 1996. Stretched exponential relaxation in molecular and electronic glasses. Rep. Prog. Phys. 59, 1133–1207.

Phillips, J.C., 2000. Microscopic theory of atomic and electronic stretched exponential relaxation in high temperature superconductors. Physica C 340, 292–298.

Sattler, R., Tymianski, M., 2001. Molecular mechanisms of glutamate receptor-mediated excitotoxic neuronal cell death. Mol. Neurobiol. 24, 107–129.

Shlesinger, M.F., Montroll, E.W., 1984. On the Williams–Watts function of dielectric relaxation. Proc. Natl Acad. Sci. USA 81, 1280–1283.

Soto, C., 2003. Unfolding the role of protein misfolding in neurodegenerative diseases. Nat. Rev. Neurosci. 4, 50–60.

Valko, P.P., Vajda, D.A., 2002. Inversion of noise-free Laplace transforms: towards a standardized set of test problems. Inverse Probl. Eng. 10, 467–483.

Vreugdenhil, E., de Kloet, E.R., Schaaf, M., Datson, N.A., 2001. Genetic dissection of corticosterone receptor function in the rat hippocampus. Eur. Neuropsychopharm. 11, 423–430.

Weibull, W., 1951. A statistical distribution function of wide applicability. J. Appl. Mech. 18, 293–297.